Multiobjective Optimization of Simulated Countercurrent Moving Bed Chromatographic Reactor (SCMCR) for MTBE Synthesis

Zhang Ziyang, K. Hidajat, and Ajay K. Ray*

Department of Chemical and Environmental Engineering, National University of Singapore, 10 Kent Ridge Crescent, Singapore 119260

The paper addresses the multiobjective optimization of a simulated moving-bed chromatographic reactor (SCMCR). The selection of the operating parameters such as the length and number of columns, switching time, and liquid flow rates in different sections is not straightforward in an SCMCR. In most cases, conflicting requirements and constraints govern the optimal choice of the decision (operating or design) variables. A mathematical model that predicts single-column experimental results well was modified for MTBE synthesis in an SCMCR. Thereafter, a few simple multiobjective optimization problems were solved that included both existing and design-stage SCMCRs using a nondominated sorting genetic algorithm (NSGA). Optimal design and operating conditions for three cases of practical relevance are studied in this work, namely, (a) simultaneous maximization of the purity and yield of MTBE; (b) simultaneous maximization of the purity and yield of MTBE, together with minimization of the total amount of adsorbent/catalyst required; and (c) maximization of the purity of MTBE with simultaneous minimization of the eluent consumption, to illustrate the procedures and interpret the results obtained. Pareto-optimal solutions were obtained in all cases, and moreover, it was found that the performance of the SCMCR could be improved significantly under optimal operating conditions.

Introduction

Simulated moving-bed (SMB) technology is receiving increasing interest as an alternative technique and has recently been widely applied in the petrochemical, biochemical, and fine chemical industries. Recent results have demonstrated the efficiency of this technology for use both as separators and as reactor−separators. As in reactive distillation, which couples distillation and chemical reaction together in one process, simulated countercurrent moving-bed chromatographic reactor (SCMCR) technology combines the more powerful and energy-saving separation technology of an SMB with a reversible chemical reaction in one reactor.

In the simulated system, a fixed bed is used, and the countercurrent movement is simulated by successive switching, at timed intervals, of the feed position through a series of inlets located at intervals along a single column[1] or between a series of packed columns.[2] The shifting of the feed and the product positions in the direction of the fluid flow mimics the movement of solids in the opposite direction. For all practical purposes, simulated countercurrent operation is continuous in that the rates and compositions of all streams entering and leaving the adsorbent bed are continuous functions without the associated problems of actual conveyance of solids. This eliminates the problem of solids handling, fines removal, solids recycling, and flow channeling that are usually encountered in traditional moving beds. In addition to the economic advantage gained by integrating the reactor and separator into one unit, SCMCR also enhances the conversion, yield, selectivity, and purity of the desired product beyond the levels predicted by thermodynamics for an equilibrium-limited reversible reaction.

* Corresponding author. Tel.: +65 6874 8049. Fax: +65 6779 1936. E-mail: cheakr@nus.edu.sg

The design of a simulated moving-bed system is associated with several important objectives that require optimization, along with many constraints that must be satisfied at the same time. Rigorous optimal designs of SCMCRs would help in further increasing their competitiveness. Unfortunately, not much work has been reported in the open literature on the multiobjective optimization of SCMCR systems. To the best of our knowledge, this is the first attempt at addressing such a problem. In this paper, we select one simple representative example from among a whole variety of reactions that can be studied in SCMCR systems, namely, the optimization of MTBE synthesis. The method of optimization used in this work is very general and can easily be applied to almost any other systems including separations (e.g., chiral separation) only. We illustrate the procedure to be used and present solutions of a few relatively simple optimization problems with two objective functions and a few constraints. A whole variety of other problems can, indeed, be formulated and solved, depending upon one's interest.

Recently, we studied synthesis of methyl tertiary butyl ether (MTBE) by the direct etherification reaction between methanol and tertiary butyl alcohol (TBA) on acid ion-exchange resin, Amberlyst 15.[3] Subsequently, we developed a mathematical model for the MTBE synthesis reaction in an SCMCR system.[4] The mathematical model can predict concentration profiles of the reactant, TBA, and products, MTBE and H_2O. It was observed that MTBE travels faster than H_2O; separation at the site of reaction to increase the yield, selectivity, and purity of MTBE is possible; and the SCMCR configuration reaches a pseudo-steady state after 100 switching operation. The switching time and solvent flow rate play very important roles in achieving an effective separation between the components in SCMCRs. The effect of the feed, solvent, and product flow

10.1021/ie0106940 CCC: $22.00
Published on Web 06/04/2002

rates; the switching time; and the number of columns in the SCMCR configuration on the concentration profiles of the three components; the yield, selectivity, and purity of MTBE at the raffinate port; and the conversion of the limiting reactant, TBA, were studied. It was found that some of the process parameters not only alter the yield, selectivity, and purity of MTBE profoundly, but also act in a conflicting manner. Moreover, it is not possible to maximize the yield and selectivity simultaneously. By adjusting process parameters, it is possible to reach a conversion of TBA and a selectivity and purity of MTBE as high as 98%, as well as a yield of MTBE as high as 95%, although not all simultaneously. This is in contrast to equilibrium conversion, yield, selectivity, and purity of 85.3, 76.1, 47.2, and 43.2%, respectively. The reported results[3] were obtained by sensitivity analysis (simulation−optimization) without actual optimization of the entire process. Further improvement is expected if a systematic process optimization is conducted using multiple objectives.

In this work, multiobjective Pareto-optimal solutions are generated for use in the design and operation of the direct synthesis of MTBE in an SCMCR using a genetic algorithm (GA). GA is a nontraditional search and optimization method[5−8] that has become quite popular in engineering optimization. It mimics the principles of genetics and the Darwinian principle of natural selection (i.e., survival of the fittest). A simple genetic algorithm (SGA) is suitable for optimizing problems with a single objective function. In single-objective-function optimization, one attempts to find the best design, which is usually the global minimum (or maximum). However, most real-world problems involve the simultaneous optimization of multiple objective functions (a vector). Such problems are conceptually different from single-objective-function problems. In multiple-objective-function optimization, a solution that is the best (global optimum) with respect to all objectives might not exist. Instead, an entire set of optimal solutions might be equally good. These solutions are known as Pareto-optimal (or nondominated) solutions. A Pareto set, for example, for a two-objective-function problem is described by a set of points such that, when one moves from one point to any other, one objective function improves while the other worsens. Thus, one cannot say that any one of these points is superior (or dominant) to any other. Because none of the nondominated solutions in the Pareto set is superior to any other, any one of them is an acceptable solution. The choice of one solution over another requires additional knowledge of the problem, and often, this knowledge is intuitive and nonquantifiable.

Several methods are available to solve multiobjective optimization problems, e.g., the ϵ-constraint method,[9] goal-attainment method,[10] and the nondominated sorting genetic algorithm (NSGA).[11] In this study, we use the NSGA to obtain the Pareto set. This technique offers several advantages[12] and has been applied recently to the optimization of several processes of industrial importance in chemical engineering, including an industrial nylon-6 semibatch reactor,[13] a wiped-film polyester reactor,[14,15] a PMMA reactor,[16] a steam reformer,[17] a hydrogen plant,[18] cyclone separators,[19] and membrane separation modules.[20]

Direct Synthesis of MTBE

MTBE is currently the most important high-octane blending oxygenate for gasoline, which helps motor vehicles fuel burn more cleanly by replacing toxic additives such as lead compunds. Recently, we considered the direct synthesis of MTBE by reacting *tert*-butyl alcohol (TBA) with methanol.[3,4] Amberlyst 15 ion-exchange resin was used, which acts as both a catalyst and an adsorbent for the etherification reaction in the SCMCR. The overall reaction can be described by the equation

$$n(CH_3)_3COH + CH_3OH \rightleftharpoons (CH_3)_3COCH_3 + nH_2O + (n-1)(CH_3)_2CCH_2 \quad (1)$$

where n (usually greater than 1) is an unknown parameter that indicates the amount of isobutene produced. It should be noted that, although methanol is one of the reactants, it also acts as a carrier solvent and is usually present in excess. Experiments were conducted at different temperatures, flow rates, and feed concentrations in a single packed column, and the elution (breakthrough) profiles of the various components from the exit of the column were monitored continuously. The kinetic parameters and adsorption equilibrium constants, as well as the dispersion coefficients of TBA, MTBE, and H_2O in methanol, were obtained by minimizing the error between the experimental and model-predicted results, and the results are given in the Appendix for three different temperature values. The details are described elsewhere.[3]

Synthesis of MTBE in an SCMCR

Figure 1 shows a schematic diagram of an SCMCR and the principle of its operation. It consists of a number of columns of uniform cross section, each of length L and packed with the ion-exchange resin, which acts as both a catalyst and an adsorbent. The columns are connected in series in a circular array. Two incoming fluid streams (feed and eluent/desorbent) and two outgoing fluid streams (extract and raffinate) divide the reactor system into four sections (P, Q, R, and S), where p, q, r, and s represent the number of columns in each section, respectively, as illustrated in Figure 1. Q_p, the flow rate in section P, is regarded as the reference flow rate, in terms of which all other flow rates are described. If α, β, and γ are assumed to be the ratios of the feed flow rate (F), raffinate flow rate (Ra), and eluent flow rate (E), respectively, to the reference flow rate, Q_p, then the flow rates in each section can be defined as shown in Figure 1. Simulation of the countercurrent movement of the solid is achieved by advancing the inlet and withdrawal ports, column by column, in the same direction as the fluid flow, at the predetermined switching time t_s. However, to achieve separation between the components, the internal flow rates of the fluid phases within the four sections and the switching time (which defines the hypothetical solid-phase velocity) have to be specified appropriately. For a true countercurrent moving-bed chromatographic reactor (CMCR), Petroulas and co-workers[21] defined a parameter, σ_i, called the relative carrying capacity of the solid relative to the fluid stream for any component i, as

$$\sigma_i = (1 - \epsilon/\epsilon)NK_i(u_s/u_g) = \delta_i(u_s/u_g) \quad (2)$$

They showed that, to achieve countercurrent separation between two components, one must set σ greater than 1 for one component and less than 1 for the other. Fish and co-workers[22] defined V_i, the net velocity at which

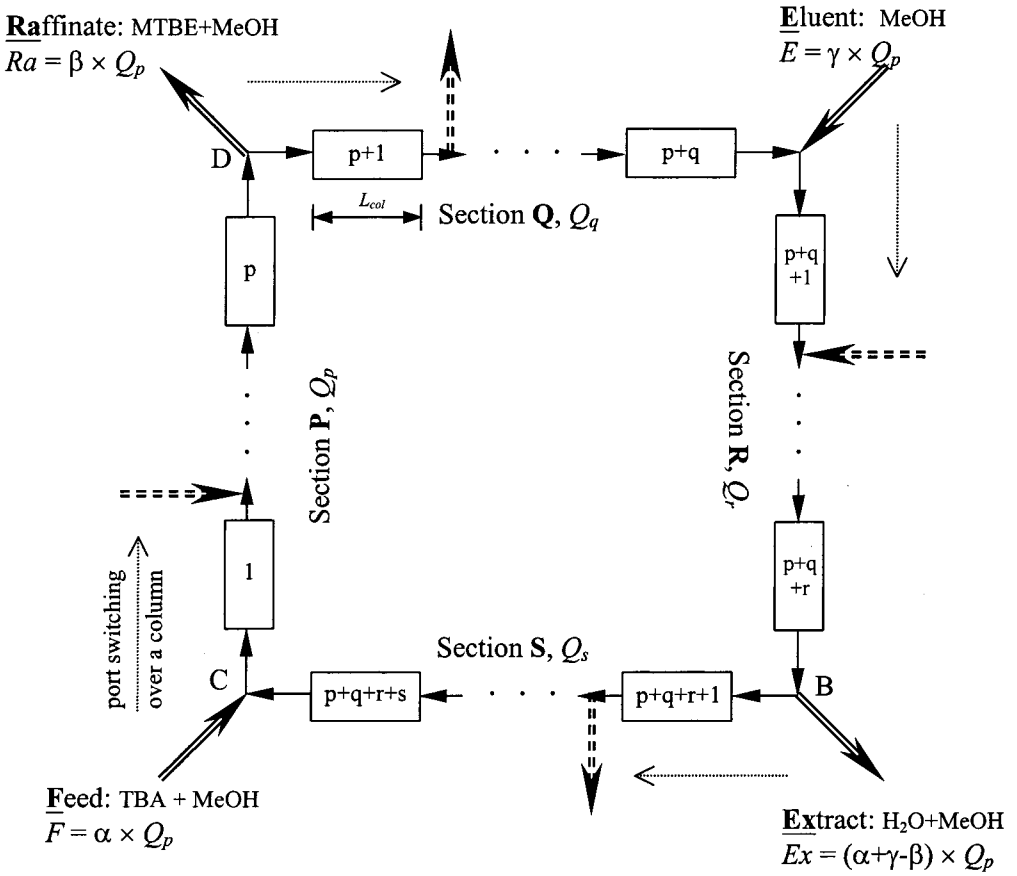

Figure 1. Schematic flow diagram of the SCMCR. The inlets and outlets divide the entire system into four sections, P, Q, R, and S, with *p*, *q*, *r*, and *s* columns, respectively. The flow rates in the different sections are given by $Q_q = (1 - \beta)Q_p$, $Q_r = (1 - \beta + \gamma)Q_p$, and $Q_s = (1 - \alpha)Q_p$, where α, β, and γ are given by F/Q_p, Ra/Q_p, E/Q_p, respectively.

component *i* travels (or the concentration front moves) within the column, which for a linear isotherm is given by

$$V_i = [u_g(1 - \sigma_i)/(1 + \delta_i)] \quad (3)$$

Therefore, when $\sigma_i < 1$, $V_i > 0$ (species move with the fluid phase), and when $\sigma_i > 1$, $V_i < 0$ (species move with the solid phase). $\sigma = 0$ represents fixed bed. Ray and co-workers[23] redefined the above parameter σ for SCMCRs by replacing the solid-phase velocity, u_s, in the CMCR by a hypothetical solid-phase velocity ζ, defined as $\zeta = L/t_s$, for the SCMCR. They found, both theoretically[1] and experimentally,[24] that simulation of the countercurrent movement between two components can be achieved when the redefined σ's were set such that the value was greater than 1 for one component and less than 1 for the other. Hence, in the present study, if we set σ properly, the more strongly adsorbed component (H_2O) will move with the solid (resin) stream and can be collected at the extract port (point B in Figure 1), while at the same time, the less strongly adsorbed component (MTBE) will travel with the fluid stream and can be collected at the raffinate port (point D in Figure 1). It should also be noted that the parameter σ defined by the research group of Carr and Aris[21] is similar to β defined by the research group of Hashimoto,[25] γ defined by the research group of Ruthven,[26] and *m* defined by the research group of Morbidelli.[27]

The mathematical model for the SCMCR used in this study is identical to that reported earlier.[4] Because the mathematical model and simulation of the SCMCR are thoroughly described in ref 4, the same level of detail is not included here for brevity. However, for completeness, the full set of equations is provided in the Appendix. The mass balance equation (eq A1), initial (eqs A4 and A5) and boundary (eqs A6−A9) conditions, kinetic equation (eq A2), and adsorption isotherm (eq A3) completely define the SCMCR system. The PDEs were solved using the method of lines. The PDEs were first discretized in space using the finite difference method (FDM) to convert them into a set of several coupled ODE−IVPs, and the resultant stiff ODEs of the initial value kind were solved using the subroutine DIVPAG in the IMSL library. Because periodic switching is imposed on the system, the reactor works under transient conditions. Whenever switching is performed, a new initial value problem must be solved. However, a cyclic (periodic) steady state with a period equal to the switching time is eventually attained. After each switching, column numbering was redefined according to eq A10 so that feed is always introduced into the first column. The mathematical model is solved using experimentally determined adsorption and kinetic parameters given in the Appendix for the etherification reaction. The model can also predict the concentration profiles of the reactant (TBA) and products (MTBE and H_2O). It was observed that the SCMCR configuration reaches a pseudo-steady state after 100 switching operations and that enhancement of the yield and selectivity of MTBE is possible through the separation of the products at the site reaction.

The design of the SCMCR configuration and operating conditions to be used therein are set such that the conversion of the limiting reactant TBA (X_{TBA}) and the yield (Y_{MTBE}), purity (P_{MTBE}), and selectivity (S_{MTBE}) of the desired product (MTBE) are maximized at the raffinate port. The four quantities are defined as follows:

$$X_{TBA} = \frac{(\text{TBA fed} - \text{TBA collected in the raffinate and extract})}{\text{TBA fed}}$$

$$= \frac{\alpha C_{TBA,f} t_s - [\beta \int_0^{t_s} C^{(N)}_{TBA,p}|_{z=L}\, dt + (\alpha + \beta - \gamma)\int_0^{t_s} C^{(N)}_{TBA,p+q+r}|_{z=L}\, dt]}{\alpha C_{TBA,f} t_s} \quad (4)$$

$$Y_{MTBE} = \frac{\text{MTBE collected}}{\text{TBA fed}}$$

$$= \frac{\beta(\int_0^{t_s} C^{(N)}_{MTBE,p}|_{z=L}\, dt)}{\alpha C_{TBA,f} t_s} \quad (5)$$

$$P_{MTBE} = \frac{\text{MTBE collected}}{(\text{MTBE} + H_2O + \text{TBA})\ \text{collected}}$$

$$= \frac{\int_0^{t_s} C^{(N)}_{MTBE,p}|_{z=L}\, dt}{\int_0^{t_s} (C^{(N)}_{MTBE,p} + C^{(N)}_{H_2O,p} + C^{(N)}_{TBA,p})|_{z=L}\, dt} \quad (6)$$

$$S_{MTBE} = \frac{\text{MTBE collected}}{(\text{MTBE} + H_2O)\ \text{collected}}$$

$$= \frac{\int_0^{t_s} C^{(N)}_{MTBE,p}|_{z=L}\, dt}{\int_0^{t_s} (C^{(N)}_{MTBE,p} + C^{(N)}_{H_2O,p})|_{z=L}\, dt} \quad (7)$$

The effects of the switching time (t_s); the numbers of columns (p, q, r, and s) in sections P, Q, R, and S, respectively; and the feed (α), product (β), and solvent (γ) flow rates on the yield, selectivity, and purity of MTBE and the conversion of the limiting reactant TBA were studied. In Table 1 are shown the results of a sensitivity study of these parameters on Y_{MTBE}, S_{MTBE}, P_{MTBE}, and X_{TBA} at 328 K for a carrier flow rate (Q_p) of 1.67×10^{-8} m^3/s. For each row of Table 1, the parameter in the right-hand column denotes the x-axis variable for the corresponding plots, while the number in parentheses indicates the reference value of that parameter used in the simulation runs for the other rows. The effects of each parameter on Y_{MTBE}, P_{MTBE}, X_{TBA}, and S_{MTBE} are shown for reference values of the other parameters in the four subsequent columns. The effect of the switching time, t_s, is shown in the diagrams in the first row. Subsequently, three values of t_s (600, 780 and 1080 s) were used to show the influence of a particular parameter on Y_{MTBE}, P_{MTBE}, X_{TBA}, and S_{MTBE}. Table 1 shows that q and r, which represent numbers of columns in sections Q and R, respectively, have no impact on the final results, when each of them is varied between 1 and 6. In contrast, the switching time and solvent flow rate play a crucial role in achieving an effective separation between the components. It was found that some of the process parameters not only alter the yield, selectivity, and purity of MTBE profoundly, but also act in a conflicting manner. For example, parameters such as β and γ have a conflicting influence on the yield and purity (or selectivity) of MTBE. Furthermore, depending on t_s, the effects of α, β, γ, and p are quite different. The influence of t_s is particularly complex. Its optimum value depends not only on the distribution of columns in sections P and S, but also on the values of α, β, and γ. It is not possible to maximize the yield and selectivity simultaneously. One must perform a multiobjective optimization to determine the optimal conditions and configuration of the SCMCR. It is also to be noted that the optimum process design for an SCMCR is almost impossible (and time-consuming) to determine by simulation alone because of the large number of interrelated but conflicting parameters. In particular, when a chemical reaction is involved, new factors must also be taken into consideration. The optimization can not only provide the optimum operating conditions for the desired objectives, but also help elucidate the roles of each parameter in the SCMCR system.

Optimization of the SCMCR

In the open literature, many investigations of SCMCRs can be found, but there are still no reported industrial application of this technology, probably because of the complexity of the process and the absence of any general guidelines for the design of the process. Most of the design approaches are not based on systematic and rigorous mathematical optimization methods. The only optimization study reported on an SCMCR system was by Dünnebier and co-workers.[28] They minimized a generalized cost function with constraints on the product quality (purity) requirements of the raffinate and extract streams. They used a staged sequential optimization algorithm for the solution of the dynamic optimization problem and reported results for two different case studies, namely, the enzymatic inversion of sucrose and the production of β-phenethyl acetate. In recent years, an extremely robust technique, the genetic algorithm (GA),[5−8] as well as its adaptations [11,13] for more useful but complex multiobjective optimization problems, has become popular. GA-based approaches do not require any initial guesses and converge to the global optimum even when several local optima are present. GA uses a population of several points simultaneously and also works with probabilistic (rather than deterministic) operators. In addition, GA uses information on the objective function and not its derivatives.

In the present study, we report work on the multiobjective optimization of the complex chemical processes involved in a simulated countercurrent moving-bed chromatographic reactor (SCMCR). For the proper design of a SCMCR, and more importantly, for an understanding of the principles of operation of a SCMCR, a multiobjective optimization study is much more meaningful. To the best of our knowledge, this is the first attempt at a multiobjective optimization study of simulated moving-bed reactor systems.

Formulation of Multiobjective Optimization

An SCMCR process can be optimized for different objectives, including minimization of the fixed costs (e.g., equipment such as the total number of columns or the volume of the stationary phase) or operating costs (e.g., reactants or desorbent) and/or maximization of the throughput (feed) or product quality (e.g., purity of the product streams). However, cost data is site-specific (and

Table 1

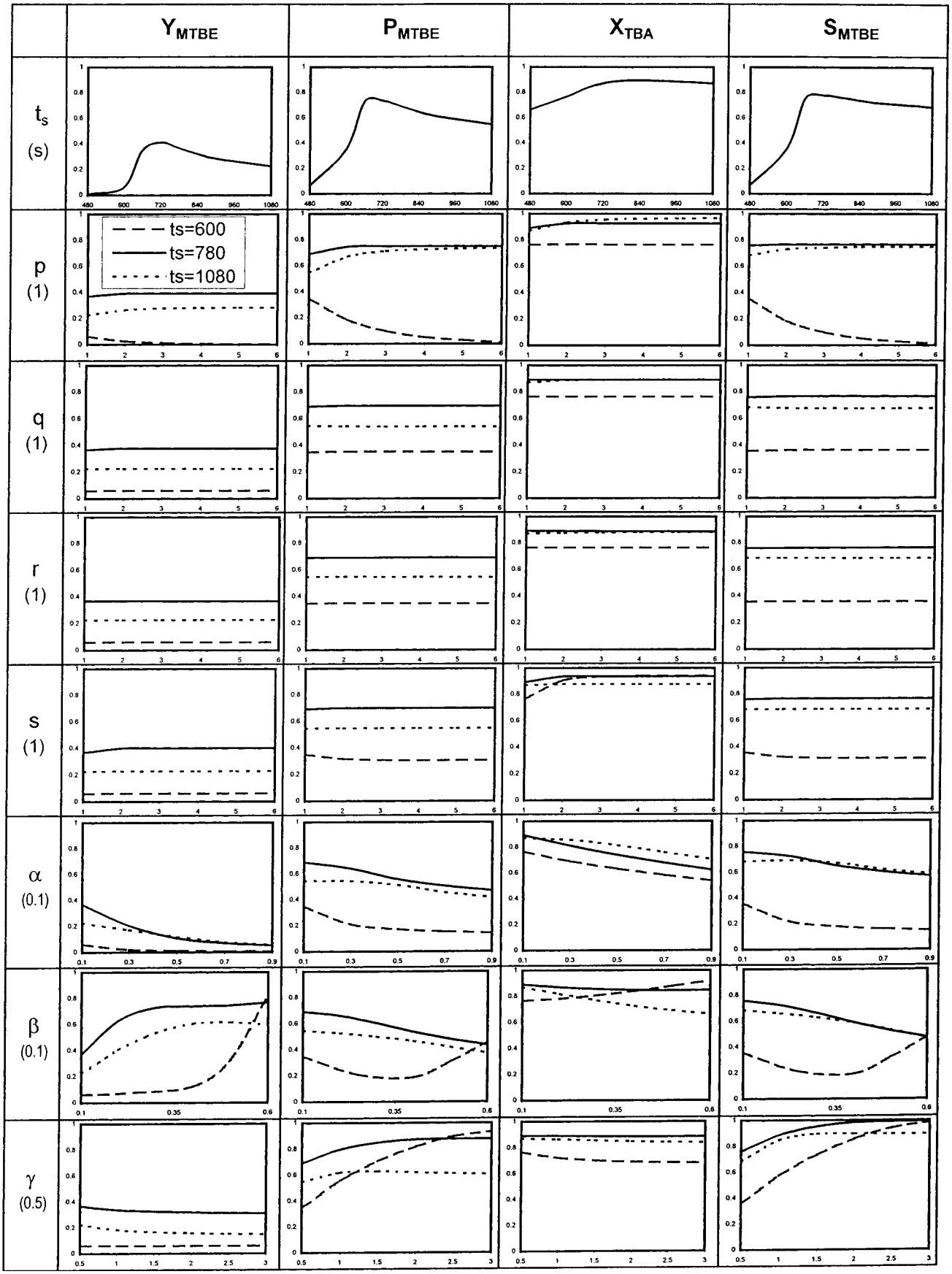

time-dependent) and, therefore, might not always provide a meaningful objective function. In an SCMCR, unlike in an SMB process for separation only, there is usually only one desired product, which is withdrawn from either the raffinate or the extract port. Therefore, in an SCMCR, the objectives usually include maximiza-

Table 2. Description of the Optimization Problem Solved in Case 1, Together with Bounds of Decision Variables and Other Parameter Values Used in This Study

problem no.	1 reference	2 effect of α	3 effect of γ	4 effect of Q_p	5 effect of L_{col}	6 effect of N_{col}	7 effect of T
objective 1				max Y_{MTBE}			
objective 2				max P_{MTBE}			
constraint				$X_{TBA} \geq 90\%$			
t_s, min				$5 \leq t_s \leq 20$			
β				$0.05 \leq \beta \leq 0.90$			
p				$1 \leq p \leq 4$			
α	0.1	0.2, 0.5	0.1	0.1	0.1	0.1	0.1
γ	0.8	0.8	1.2, 1.6	0.8	0.8	0.8	0.8
Q_p, mL/min	1	1	1	0.694,1.694	1	1	1
L_{col}, cm	25	25	25	25	15, 35	25	25
N_{col}	7	7	7	7	7	4, 6, 8	7
T, K	328	328	328	328	328	328	318, 323
q				1			
r				1			
d_{col}, cm				0.94			
figure no.	2	4	6	5	7	8	9

tion of the yield, purity, or selectivity of the desired product and/or the conversion of the limiting reactant. One can also consider an objective function such as maximization of the throughput (capacity) or minimization of the desorbent (eluent). It is possible to consider all of these objective functions together, but it can be difficult to analyze the optimum solutions in such cases, as one has to consider multidimensional surfaces. Hence, in this paper, we illustrate the procedure to be used and present solutions of a few relatively simple optimization problems with two objective functions and a few constraints. A whole variety of other problems can, indeed, be formulated and solved, depending upon one's interest. The method of optimization used in this work is very general and can easily be applied to almost any other combinations of objective functions.

For the synthesis of MTBE in an SCMCR, the decision variables can be classified as (a) fixed cost parameters, including the total number of columns (N_{col}), and length (L_{col}) and diameter (d_{col}) of each column; (b) operating cost parameters, such as the temperature (T), eluent flow rate (γ), and maximum flow rate of the carrier (Q_p), which is related to the maximum pressure drop in the system; (c) throughput parameters, including the feed flow rate (α) and the MTBE flow rate from the raffinate port (β); and (d) process parameters, including the switching time (t_s), and the distribution of columns in sections P, Q, R, and S (p, q, r, and s, respectively).

The first multiobjective optimization problem (case 1) solved is for an existing setup and is described mathematically by

$$\max J_1 = Y_{MTBE}(t_s,p,\beta) \tag{8a}$$

$$\max J_2 = P_{MTBE}(t_s,p,\beta) \tag{8b}$$

subject to

$$X_{TBA} \geq 90\% \tag{8c}$$

$$N_{col} = 7,\ L_{col} = 25\ \text{cm},\ d_{col} = 0.94\ \text{cm},\ T = 328\ \text{K}$$

$$\alpha = 0.1,\ Q_p = 1\ \text{mL/min},\ \gamma = 0.8,\ q = r = 1 \tag{8d}$$

$$\text{model eqs described in the Appendix} \tag{8e}$$

The choice of the two objective functions, J_1 and J_2, in eqs 8a and 8b enables the simultaneous maximization of the yield and purity of the desired product, MTBE. These two objective functions were chosen as the primary goal of MTBE synthesis in the SCMCR. We reported in our earlier paper[4] that the direct synthesis reaction of MTBE is not severely equilibrium-limited, as the equilibrium conversion of TBA in a nonseparative reactor can reach as high as 85% at 328 K (see the Appendix). However, in an SCMCR, an even higher value for the conversion of TBA can be achieved if the operating conditions are set properly. Hence, we have incorporated an inequality constraint to achieve conversions of TBA greater than 90%. It should also be noted that maximization of P_{MTBE} simultaneously maximizes S_{MTBE}, as the effects of different parameters on these two functions are always in the same direction (see Table 1). Moreover, with a high desired conversion of TBA and a low TBA feed concentration, the difference between P_{MTBE} (eq 6) and S_{MTBE} (eq 7) is expected to be very small. The inequality constraint (eq 8c) was incorporated using penalty functions. Because the optimization code was developed for minimization of a function, the optimization problem (eqs 8a−8c) was rewritten as the minimization problem

$$\min I_1 = \left(\frac{1}{1 + J_1}\right) + wf^2 \tag{9a}$$

$$\min I_2 = \left(\frac{1}{1 + J_2}\right) + wf^2 \tag{9b}$$

where

$$f = |(X_{TBA} - 0.90)| - (X_{TBA} - 0.90) \tag{9c}$$

In eqs 9a and 9b, the large numerical weighting factor ($\sim 5.0 \times 10^4$) on the operating constraints penalizes the objectives I_1 and I_2 in the event of a constraint violation.

Three decision variables were used for the case 1 optimization study. They are the switching time (t_s), the number of columns in section P (p), and the amount of raffinate product withdrawn (β). Because an existing setup is being considered for case 1, N_{col}, L_{col}, and d_{col} were kept fixed in the reference run, as shown in Table 2. The eluent flow rate (γ), maximum column flow rate (Q_p), and temperature (T) in the columns were also kept fixed so that the optimum results at fixed operating cost could be compared. In the sensitivity analysis (see Table 1), we found that the numbers of columns in sections Q and R (see Figure 1) do not influence Y_{MTBE} and P_{MTBE}, and therefore, their values were fixed at 1. Because the total number of columns (N_{col}) is fixed, we could there-

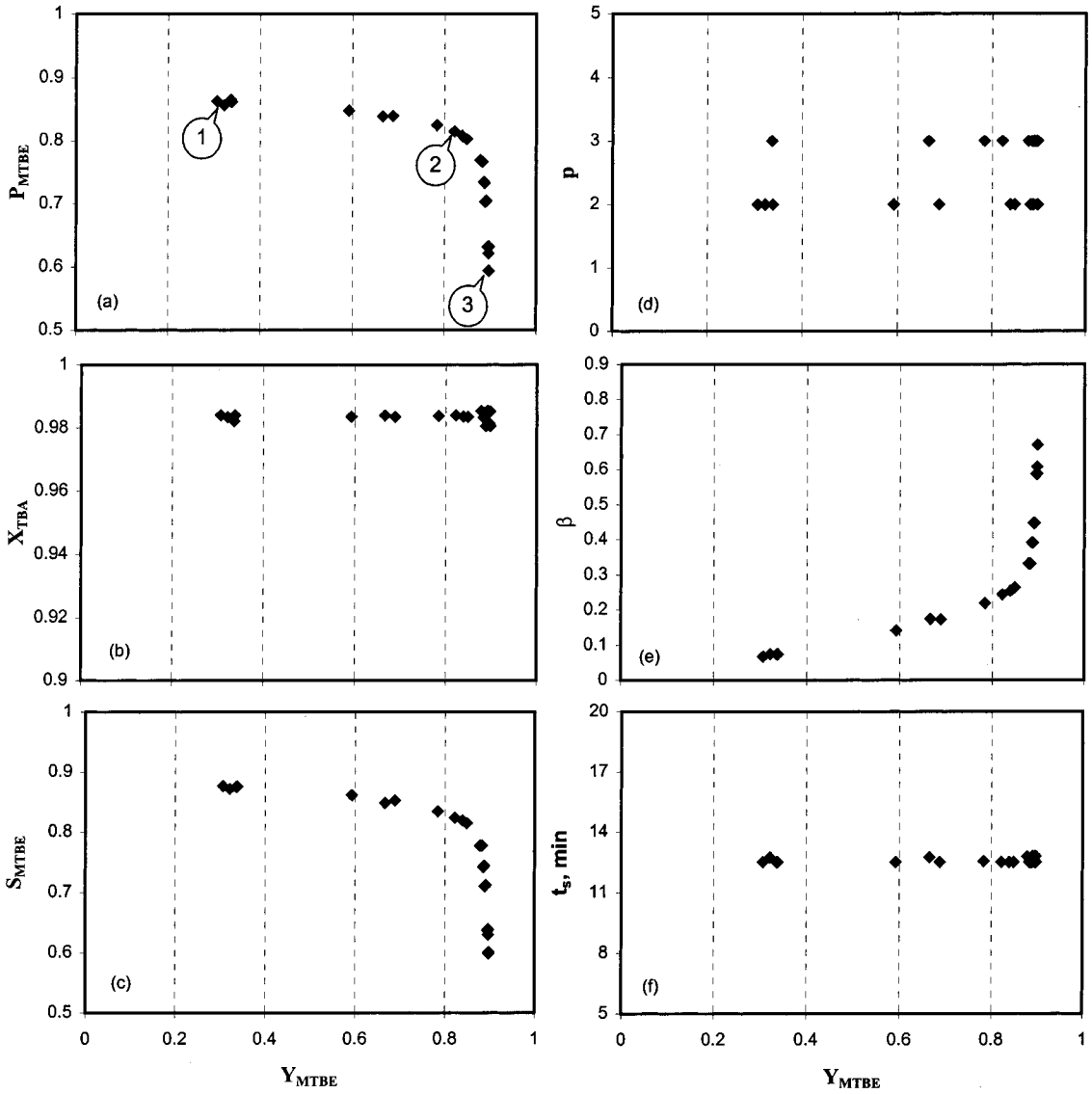

Figure 2. Pareto set for the reference run (problem 1 in Table 2) and values of X_{TBA}, S_{MTBE}, and the decision variables corresponding to the points on the Pareto set in Figure 2a.

fore independently select either p (number of columns in section P) or s (number of columns in section S) as the variable of interest. Hence, we selected p as one of the decision variables. Of the two throughput parameters (α and β), we selected β to determine the optimum raffinate flow rate (β) for a fixed feed rate (α). As the switching time (t_s) was found to be the key parameter in an SCMCR, it was selected as the third decision variable. These choices would usually be available for an existing setup. Therefore, in case 1, the optimization problem was to determine optimum values of the process parameters to maximize Y_{MTBE} and P_{MTBE} for constant fixed and operating costs and a constant throughput. However, we examine the effect (sensitivity) of some of these parameters (N_{col}, L_{col}, T, α, γ, and Q_p) on the Paretos later. The bounds of the decision variables, along with the values for the other parameters, are given in Table 2. The optimization problem was solved using an adaptation of the genetic algorithm, the nondominated sorting genetic algorithm (NSGA). Details of the NSGA are available elsewhere.[11,12]

The Pareto-optimal solution for the reference run (see Table 2), together with X_{TBA}, S_{MTBE}, and the optimal values of the three decision variables (p, β, t_s) corresponding to the points on the Pareto set, are shown in Figure 2a−f. Figure 2a shows the relation of the two objectives, P_{MTBE} and Y_{MTBE}, for case 1. The purity of MTBE at the raffinate port cannot be improved without sacrificing its yield under the same process operating conditions. The conversion of TBA was found to be approximately constant at 98%, as shown in Figure 2b, compared to the equilibrium value of 85.2%. As expected, S_{MTBE} in Figure 2c follows the same trendline as P_{MTBE}, because of the high X_{TBA} value. Each point (referred to as a chromosome) in the Pareto set (Figure 2a) is associated with a set of decision variables. Figure 2d shows that, if the total number of columns, N_{col}, and the numbers of columns in sections Q and R are fixed at 7, 1, and 1, respectively, the optimum number of columns in section P (p) is found to be either 2 or 3, which means that s is either 3 or 2. This also means that the optimum choice between the number of columns in sections P and S is insensitive to the values of Y_{MTBE} and P_{MTBE} value, as identical yield and purity values can be obtained with either $p = 2$ (and $s = 3$) or $p = 3$ (and $s = 2$). The optimum value of the switching time (t_s) was found to be constant at 12.5 min (Figure 2f). The flow rate of the raffinate stream (β) was found

Table 3. Comparison of Objective Function Values and Optimum Operating Parameters for a Few Chromosomes in the Pareto Sets Shown in Various Figures

point in figure	P_{MTBE} (%)	Y_{MTBE} (%)	t_s (min)	β	p
1 in Figure 2	86.28	30.63	12.52	0.067	2
2 in Figure 2	81.46	82.15	12.52	0.243	3
3 in Figure 2	59.34	89.73	12.52	0.671	2
4 in Figure 4	81.40	70.89	13.21	0.234	3
5 in Figure 4	75.84	69.58	19.75	0.503	4
6 in Figure 5	81.20	81.29	17.49	0.247	3
7 in Figure 5	81.79	80.88	7.48	0.228	3
8 in Figure 6	88.80	80.65	13.30	0.268	3
9 in Figure 6	95.34	80.28	17.06	0.419	4
10 in Figure 9	62.90	90.27	12.74	0.600	3
11 in Figure 9	62.49	95.57	24.29	0.640	3

to be the parameter responsible for the resulting Pareto (Figure 2e). A high value of X_{TBA} can be achieved through the in situ separation of MTBE and H_2O, and an increase in the residence time in sections P and S can be achieved through the use of more columns in these sections, where the reaction occurs.

The Pareto-optimal solution obtained can be explained by comparing the optimal operating values of the parameters P_{MTBE}, Y_{MTBE}, t_s, β, and p (Table 3), the σ and V values for the two components (MTBE and H_2O) in each section (Table 4), and the concentration profiles (Figure 3) for the three representative points 1, 2, and 3 shown in Figure 2. As we move from point 1 to point 3, Y_{MTBE} increases, but P_{MTBE} decreases. The Pareto solution obtained is mainly due to different β values, as the optimum t_s value (= 12.52 min) is the same at all three points. The different β values alter the fluid flow rates in sections Q and R, thus modifying the performance of these two sections.

Analysis of Concentration Profiles under Optimal Operating Conditions

In the four-section SMB process shown in Figure 1, all input/output ports shift by one column in the direction of fluid flow after a fixed interval (switching time, t_s). To achieve a good separation, each section should fulfill its own role, which is determined by the length and number of columns, the fluid flow rates in each section, and the switching time. The main task of section P is to retain strongly adsorbed component H_2O (adsorption of H_2O) so that it does not break through at the raffinate port where MTBE (the weakly adsorbed component) is collected as the product. Possible difficulties in this section might result from a large column fluid flow rate (Q_p), a small section length ($L_{col} \times p$), a long switching time (t_s), and axial dispersion (D). Part of the MTBE flows into section Q, where the column flow rate Q_q [= $(1 - \beta)Q_p$] should be small enough to prevent MTBE from breaking through into section R. The primary roles of section Q are, therefore, retention of MTBE and desorption of eluent (MeOH). Section R has the maximum flow rate, Q_r [= $(1 - \beta + \gamma) Q_p$], to desorb H_2O as well as MTBE so that at least the first column of this section is clean before the next port switching is done. Difficulties for this task might result from an insufficient fluid flow rate (Q_r), a short switching interval (t_s), and a large column length (L_{col}), as well as axial dispersion and the tailing effects of the desorbing concentration front. The column flow rate in section S, Q_s [= $(1-\alpha)Q_p$], is lower than Q_r after H_2O is withdrawn as a product (extract) at a rate of $Q_r - Q_s$. However, Q_s should be large enough to desorb MTBE from section S to be mixed with feed as the recycle to section P. At the same time, H_2O should be retained in section S. The difficulties for the task of this section are similar to those for section R, but the influence of axial dispersion is more significant because of the concentration shock caused by the introduction of feed at the end of section S.

The lengths of sections P and S should be large enough to prevent H_2O from breaking through at the raffinate port and into section P, respectively, as the primary objective for MTBE synthesis is to maximize the purity and yield of MTBE. The roles of sections Q and R are respectively to retain MTBE and desorb H_2O, respectively. However, because the primary objective in MTBE synthesis is not necessarily to achieve a high purity of H_2O at the extract port, the column lengths of these two sections could be small, and one column might be enough for each of these two sections. In general, when columns are of identical length (as required in the design of an SCMCR), it is advantageous for them to be smaller in length but larger in number so that the columns can be distributed in each section optimally to achieve the desired objective.

The roles of the four sections in an SMB discussed above are demonstrated by the progression of the concentration profiles of MTBE, H_2O, and TBA in Figure 3. The concentration profiles of H_2O (strongly adsorbed component primarily collected at the extract port) and MTBE (weakly adsorbed component primarily collected at the raffinate port) are shown in Figure 3 for three points (shown as 1, 2, and 3 in Figure 2) for a seven-column system during the 100th switching period. We should note that these points are only a few representative points from the infinite set of optimal solutions obtained for case 1 and shown in Figure 2. The

Table 4. Comparison of σ and V Values of the Two Components (MTBE and H_2O) in Different Sections for a Few Chromosomes in the Pareto Sets Shown in Various Figures

	section P				section Q				section R				section S			
point in figure	σ_{MTBE}	σ_{H_2O}	V_{MTBE}	V_{H_2O}	σ_{MTBE}	σ_{H_2O}	V_{MTBE}	V_{H_2O}	σ_{MTBE}	σ_{H_2O}	V_{MTBE}	V_{H_2O}	σ_{MTBE}	σ_{H_2O}	V_{MTBE}	V_{H_2O}
1 in Figure 2	0.25	2.29	1.86	−0.90	0.27	2.45	1.70	−0.95	0.14	1.32	3.69	−0.39	0.28	2.54	1.62	−0.97
2 in Figure 2	0.25	2.29	1.86	−0.90	0.33	3.02	1.26	−1.08	0.16	1.47	3.25	−0.51	0.28	2.54	1.62	−0.97
3 in Figure 2	0.25	2.29	1.86	−0.90	0.76	6.95	0.20	−1.38	0.22	2.03	2.19	−0.81	0.28	2.54	1.62	−0.97
4 in Figure 4	0.24	2.17	1.90	−0.82	0.31	2.83	1.32	−0.98	0.15	1.38	3.30	−0.42	0.30	2.71	1.40	−0.96
5 in Figure 4	0.16	1.45	2.09	−0.32	0.32	2.92	0.84	−0.67	0.12	1.12	2.83	−0.11	0.32	2.90	0.85	−0.67
6 in Figure 5	0.26	2.36	1.28	−0.66	0.34	3.13	0.85	−0.78	0.17	1.52	2.23	−0.39	0.29	2.62	1.11	−0.71
7 in Figure 5	0.25	2.26	3.17	−1.50	0.32	2.93	2.21	−1.77	0.16	1.44	5.58	−0.82	0.27	2.51	2.75	−1.62
8 in Figure 6	0.23	2.15	1.90	−0.81	0.32	2.94	1.24	−1.00	0.12	1.11	4.22	−0.15	0.26	2.39	1.65	−0.88
9 in Figure 6	0.18	1.68	2.03	−0.48	0.32	2.89	0.99	−0.77	0.08	0.77	4.96	0.35	0.20	1.86	1.78	−0.55
10 in Figure 9	0.31	2.33	1.60	−0.91	0.77	5.81	0.22	−1.32	0.26	1.94	2.06	−0.77	0.34	2.58	1.37	−0.97
11 in Figure 9	0.29	2.19	0.91	−0.45	0.80	6.09	0.09	−0.07	0.25	1.89	1.12	−0.39	0.32	2.44	0.78	−0.49
desired	<1	>1	>0	<0	>1	>1	<0	<0	<1	<1	>0	>0	<1	>1	>0	<0
	retention of H_2O				retention of MTBE				desorption of H_2O				desorption of MTBE			

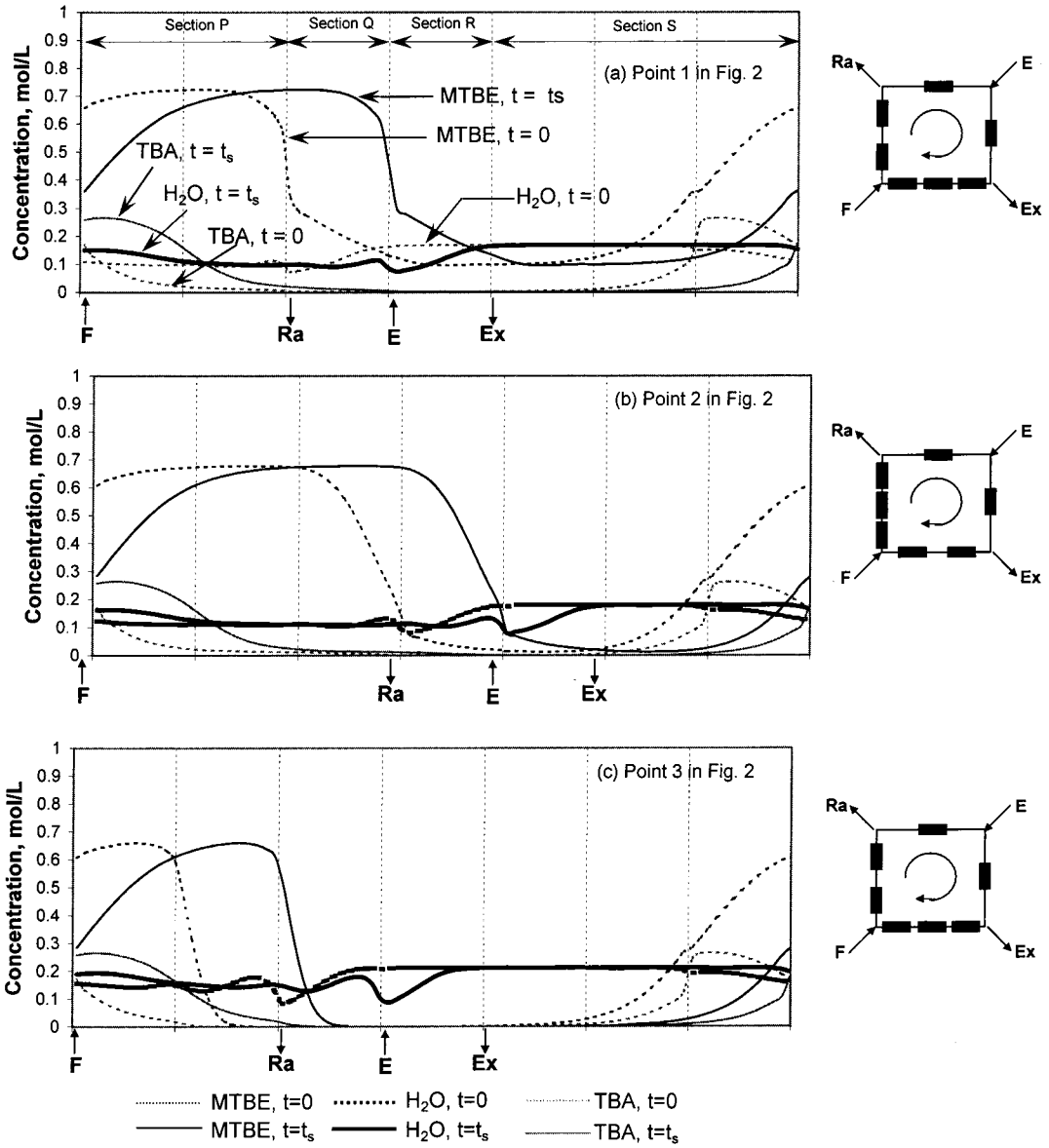

Figure 3. Concentration profiles of MTBE, H_2O, and TBA during the 100th switching period for a seven-column SCMCR corresponding to the reference run: (a) point 1, (b) point 2, and (c) point 3 shown in Figure 2a.

thick lines represent the concentration fronts of H_2O at the beginning (dotted line) and end (solid line) of the 100th switching period. Similarly, the two thin lines represent the concentration fronts of each MTBE and TBA at the beginning (dotted lines) and end (solid lines) of the 100th switching period.

As discussed earlier, the primary role of section Q is to retain MTBE (lighter component), as H_2O (heavier component) can easily be retained in section Q. Therefore, σ_{MTBE} in section Q should be greater than 1 so that MTBE travels with the solid phase, and the larger the value of σ_{MTBE}, the better. Either decreasing the switching time t_s or decreasing the fluid flow rate Q_q, or both, can achieve this end. The main role of section R is to desorb H_2O; therefore, σ_{H_2O} in this section should be less than 1 so that H_2O travels with the fluid phase, and the smaller the value of σ_{H_2O}, the better. Either increasing the switching time t_s or increasing the fluid flow rate Q_r, or both, can achieve this goal. A constant optimum t_s value (and hence a constant pseudo solid flow rate for all points) results as a compromise between the requirements of the four sections P, Q, R, and S. To achieve a high purity (by sacrificing yield) as at point 1, β must be lower than it is at point 3, where a high yield is obtained by sacrificing the purity of MTBE. When β is small, the flow rates Q_q and Q_r are large, which results in smaller values of σ_{H_2O} in section R (1.32 at point 1 compared to 2.03 at point 3 in Table 4). Therefore, H_2O is more effectively desorbed in section R, and effective regeneration of this section allows a higher MTBE purity to be obtained at the raffinate port.

Similar conclusions can be reached when reasons are sought for the high yield but low purity of MTBE at point 3. However, in this case, the performance of section Q is crucial. The higher the value of β, the lower the flow rate in section Q (Q_q), which, in turn, promotes the adsorption of MTBE in this section. Effective adsorption of MTBE in section Q prevents MTBE from eluting into section R, thereby avoiding its loss with the extract stream. This is reflected in the σ_{MTBE} values shown in Table 4 (0.76 at point 3 compared to 0.27 for point 1).

The effects of reaction and separation in an SCMCR are interrelated. On-site separation of the two products MTBE and H_2O promotes the conversion of TBA, and near-complete reaction (high X_{TBA}) favors a high MTBE

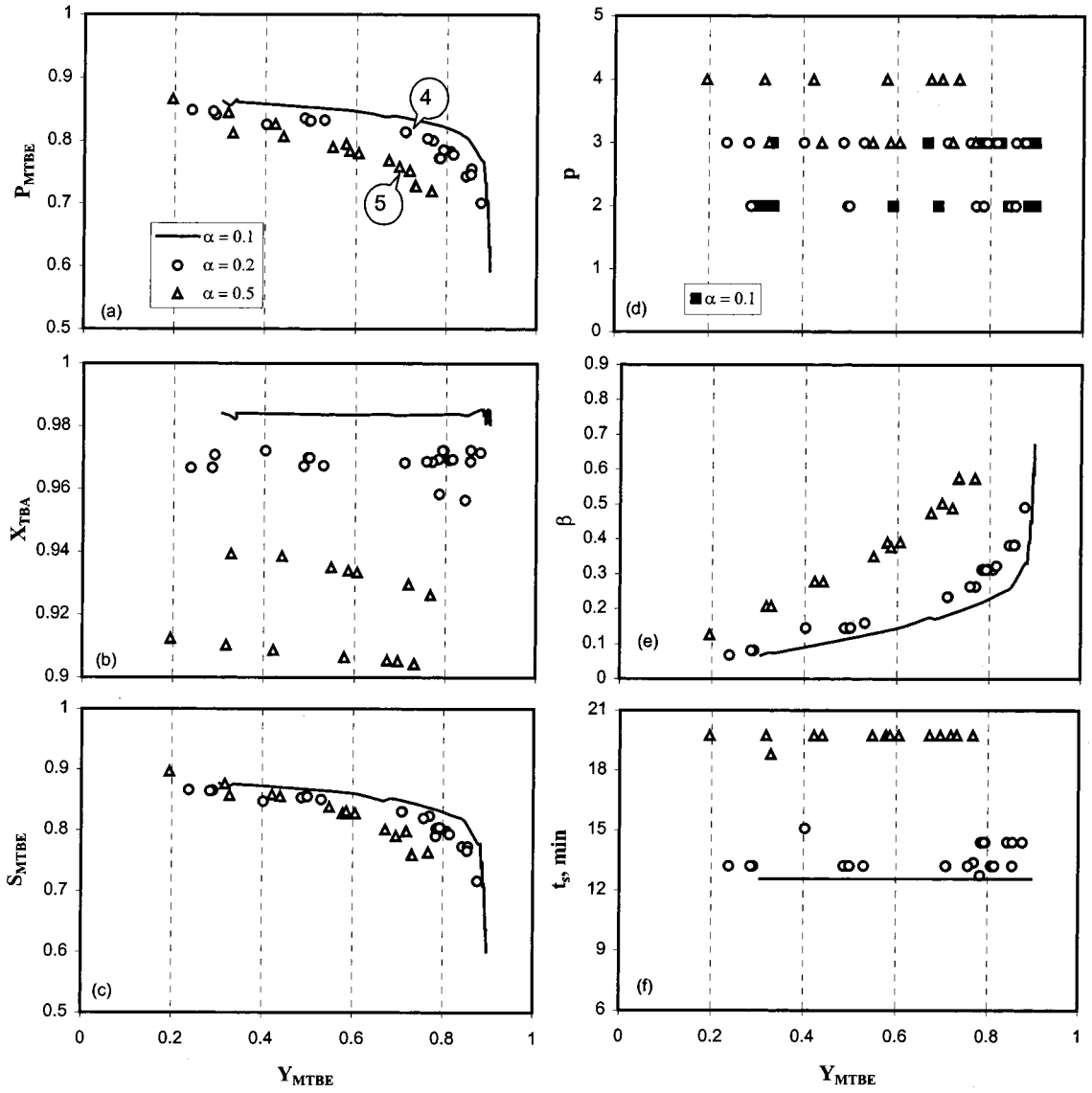

Figure 4. Effect of the feed flow rate, α, on the Pareto and the corresponding decision variables for problem 2 described in Table 2.

purity at the raffinate port. If the conversion of TBA is low, unconverted TBA is more likely to contaminate MTBE at the raffinate port. X_{TBA} is enhanced in the SCMCR through both in situ product separation and an increased residence time of TBA as the etherification reaction is kinetically controlled.

The roles played by each section can also be comprehended from the values of the parameters σ (eq 2) and V (eq 3). The values are given Table 4 for the two components (MTBE and H_2O) for each section, along with the desired values at the bottom of the table. It can be seen that equivalent countercurrent flow (true countercurrent flow in a CMCR) between the MTBE and H_2O concentration fronts occurred in sections P and S, where $\sigma_{MTBE} \leq 1$ ($V_{MTBE} \geq 0$) and $\sigma_{H_2O} \geq 1$ ($V_{H_2O} \leq 0$) for the optimal solutions (points 1−3 of Figure 2). However, in sections Q and R, equivalent countercurrent flow was not achieved even at optimal conditions because of the presence of only one column in these two sections. As a result, MTBE and H_2O accumulated at the extract and raffinate ports, respectively. It should be noted that at least two columns in each section (and a total of eight columns) are necessary to achieve countercurrent flow in an SMB unit.

Effect of Feed Flow Rate, α. Increasing the feed flow rate might increase the throughput of MTBE production, α. The sensitivity of the Pareto set was studied for two different values of α. Figure 4 compares the optimal Pareto solutions for α = 0.2 and 0.5 (problem 2 in Table 2) with that of the reference run (α = 0.1). As expected, Figure 4a−c shows that, with increasing α, the maximum obtainable Y_{MTBE}, P_{MTBE}, X_{TBA}, and S_{MTBE} values all decrease. Figure 4d shows that, when α = 0.5, the optimal column distribution between sections P and S is 4 and 1, respectively, rather than 2 and 3 (or 3 and 2) as obtained for α = 0.1 for the reference run. It is also evident that, when α increases, β (raffinate flow rate) and t_s (switching time) must also increase, as shown in Figure 4e and f, respectively. When α increases, β evidently increases as more MTBE is produced. As a result, the column flow rates in sections Q, R, and S decrease. The lower flow rate in section Q (Q_q) facilitates the performance of section Q by retaining more MTBE, thereby preventing it from breaking through into section R. However, the lower column flow rates in sections R and S decrease the performance efficiency of these two sections, as the roles of these two sections are to desorb H_2O and MTBE,

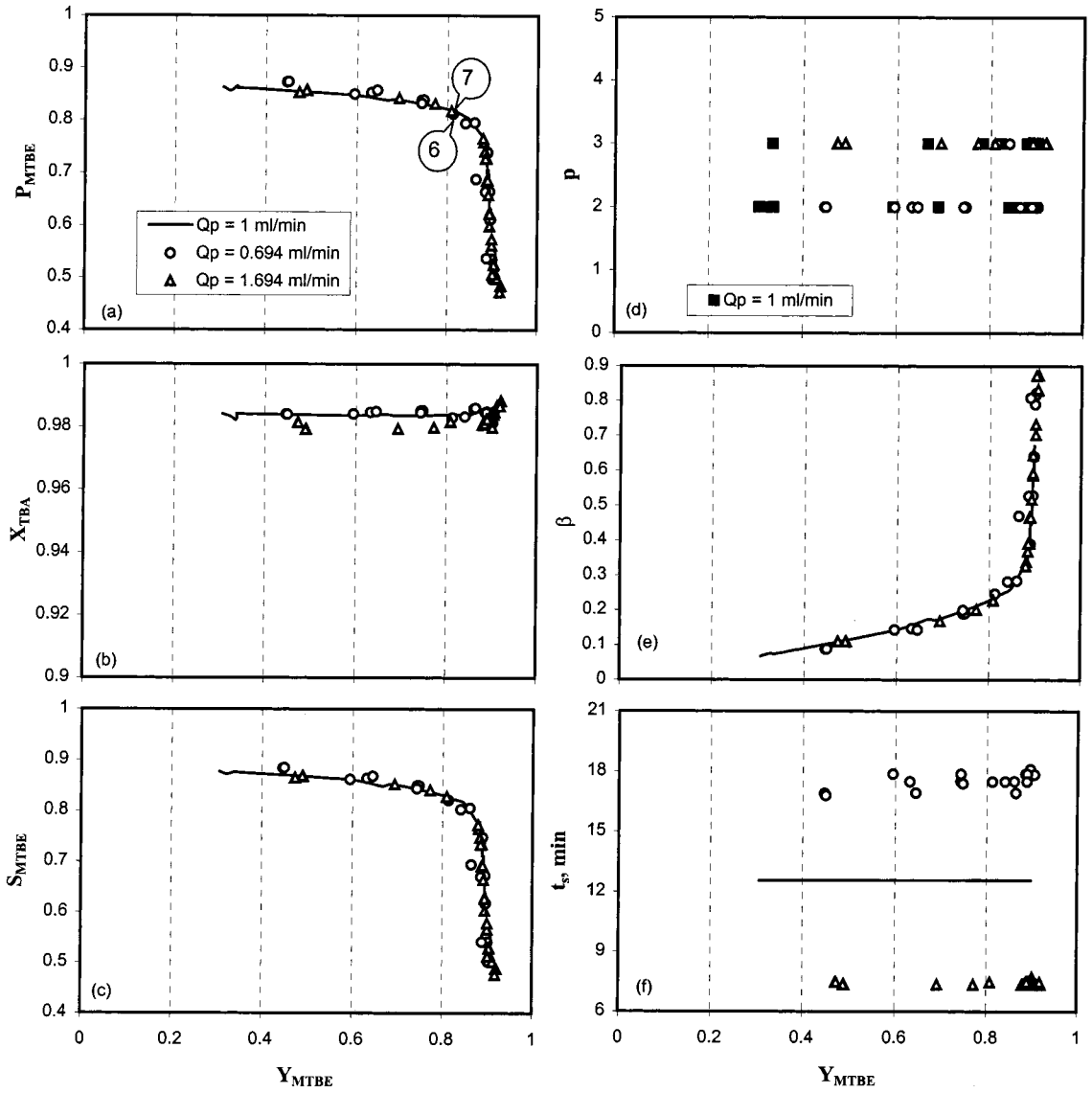

Figure 5. Effect of the column flow rate, Q_p, on the Pareto and the corresponding decision variables for problem 4 described in Table 2.

respectively. However, the decrease in the performance efficiency of sections R and S is compensated by the increase in switching time (t_s), which, in contrast, deteriorates the performance of section P, as a high switching time allows H_2O to break through and pollute the raffinate (primarily MTBE) product. To prevent H_2O from breaking through at the raffinate port, the optimal column distribution for sections P and S turns out to be 4 and 1 (note that N_{col} is fixed at 7) when $\alpha = 0.5$. Although several rearrangements in the values of the optimal decision variables took place to compensate for the impact of increasing α on the two objective functions, the reaction−separation results do decrease with increasing α, as illustrated in Table 3 for points 4 and 5 in Figure 4. Point 5 ($\alpha = 0.5$) has almost the same Y_{MTBE} value as point 4 ($\alpha = 0.2$), but its P_{MTBE} value is significantly lower. This can also be explained by comparing σ and V values shown in Table 4. For example, section P is responsible for the purity of MTBE by preventing H_2O from breaking through into the raffinate stream. For point 5, σ_{H_2O} is lower (= 1.45) than that for point 4 (= 2.17), indicating that H_2O is less efficiently retained, thereby lowering P_{MTBE}. Similarly, almost identical values for Y_{MTBE} at points 4 and 5 can be explained by the near-identical values of σ_{MTBE} in sections Q and S, as the roles for these sections are to retain and desorb MTBE, respectively. Likewise, lower values of X_{TBA} with increasing α are due to less effective separation between MTBE and H_2O, which results in an increase in the reverse reaction rate.

Effect of Flow Rate Q_p. The effect of the reference column flow rate, Q_p, on the Pareto-optimal solution is shown in Figure 5. When Q_p is increased with α and γ fixed at their reference values, the fluid-phase flow rates in all sections increase. One would expect better performance efficiency for the SCMCR, as the higher flow rate should increase the efficacy for separation of MTBE and H_2O, thereby increasing the yield and purity. However, from Figure 5a, no shift in the Pareto was observed either at lower Q_p (0.694 mL/min) or at higher Q_p (1.694 mL/min) compared to the reference value of 1 mL/min. This result can be explained easily if we look at the separation factor ($K_{H_2O}/K_{MTBE} = 9.17$), which indicates that the separation of H_2O and MTBE is easy for Amberlyst 15. As expected, the optimal column distribution between section P and S (Figure 5d) and the raffinate flow rate β (Figure 5e) are same as those in the reference run. However, the optimal t_s values (Figure 5f) are different, even though the objective function values are identical. This is because, to achieve

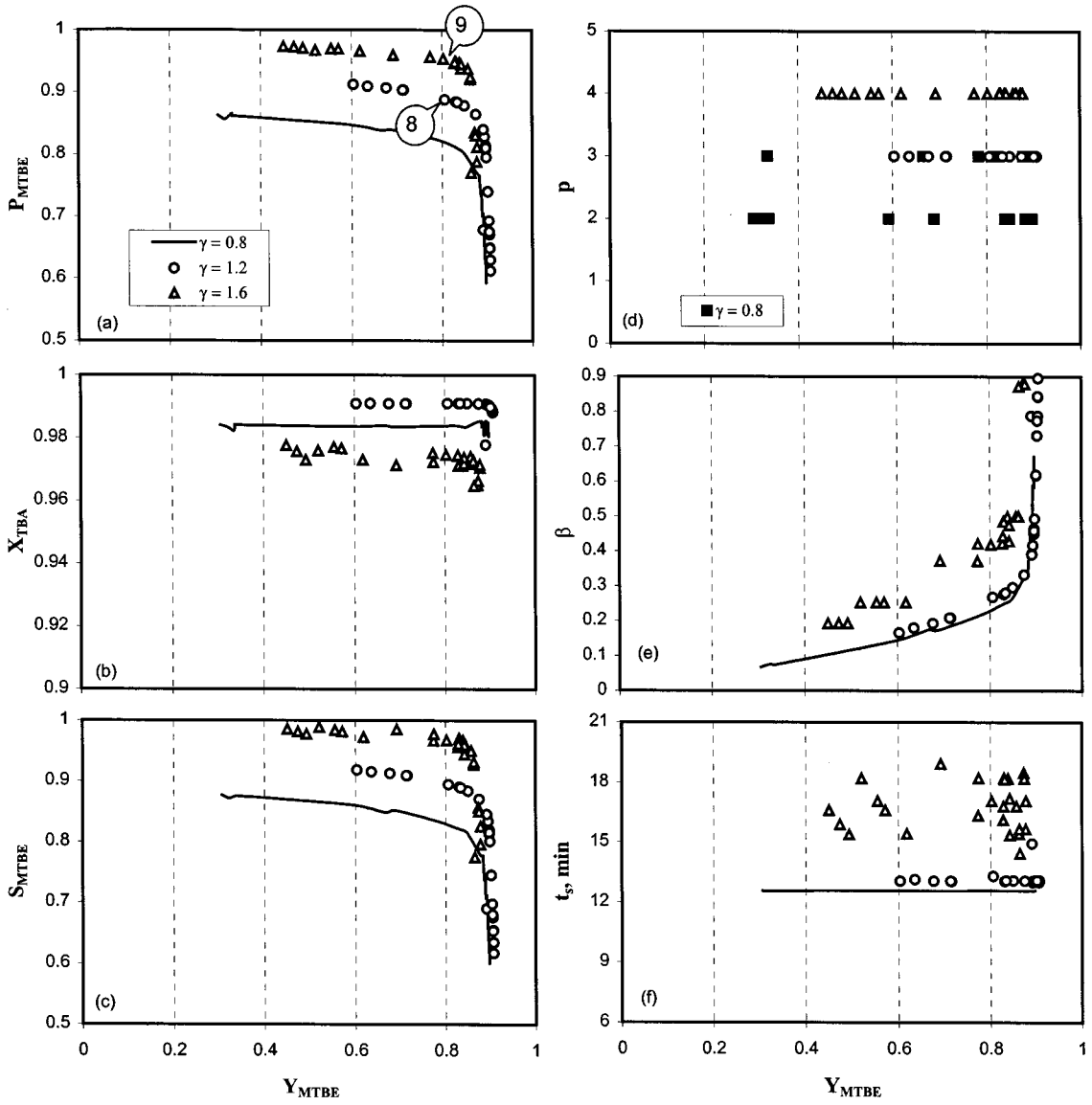

Figure 6. Effect of the desorbent flow rate, γ, on the Pareto and the corresponding decision variables for problem 3 described in Table 2.

similar performance levels (same Y_{MTBE} and P_{MTBE}), the pseudo solid flow rate must be increased when Q_p is increased, which means that the switching time must be reduced. The representative points 6 ($Q_p = 0.694$ mL/min) and 7 ($Q_p = 1.694$ mL/min) shown in Figure 5 have similar Y_{MTBE} and P_{MTBE} values, which is also reflected in the σ and V values (Table 4).

Effect of Eluent (Desorbent) Flow γ. Figure 6 shows the effect of the eluent flow rate on the shift of the optimal Pareto. A high eluent flow rate helps in effectively cleaning the columns in section R by desorbing completely the strongly adsorbed component H_2O. Effective regeneration of the columns in section R is particularly important for the H_2O/MTBE system as H_2O adsorbs strongly in Amberlyst 15. The improvement in P_{MTBE} with increasing γ is demonstrated by points 8 ($\gamma = 1.2$) and 9 ($\gamma = 1.6$) in Figure 6a. With increasing γ, the purity (as well as the selectivity) of MTBE increases for a given Y_{MTBE} as shown in Figure 6a and c. When $\gamma = 1.2$, the decision variables differ very little from their values in the reference run ($\gamma = 0.8$), except that the optimum column distribution is always $p = 3$ and $s = 2$. However, when $\gamma = 1.6$, the flow rate of the raffinate stream (β) can be large. This is accomplished with high t_s and more columns in section P ($p = 4$). A high value of γ increases the performance efficiency of section R by desorbing H_2O effectively in the extract port, which ultimately results in a high raffinate purity. However, the yield of MTBE is sacrificed, as a comparatively large portion of MTBE is removed at the extract port. One way to increase Y_{MTBE} is by increasing β, as shown in Figure 6e. However, the effect of increasing β is complex. When more MTBE is collected at the raffinate port, the flow rate Q_q [$= (1 - \beta)Q_p$] decreases, which improves the performance of section Q by preventing MTBE from breaking through into section R and averting its loss with the extract stream. However, increasing β also decreases Q_r [$= (1 - \beta + \gamma)\, Q_p$], and consequently, the performance of section R deteriorates. This is further compensated by the increase of switching time (t_s), as shown in Figure 6f. However, the increase in switching time reduces the purity of MTBE at the raffinate port. To compensate for the loss in efficiency of section P due to the increasing t_s value, the optimum number of columns in section P must be increased to 4, as shown in Figure 6d. It is intuitively anticipated that X_{TBA} should increase with an increase in γ, as the separa-

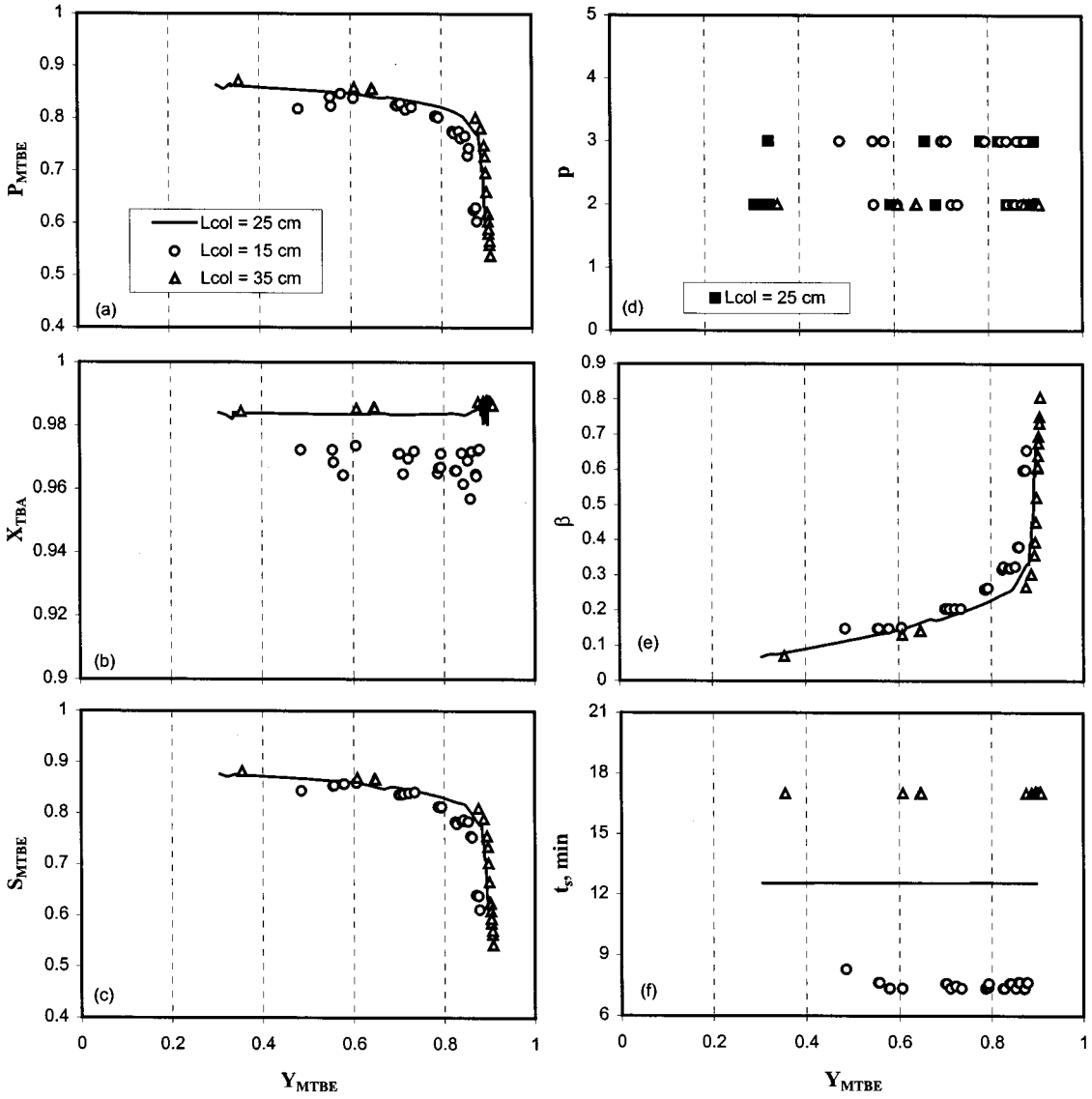

Figure 7. Effect of the column length, L_{col}, on the Pareto and the corresponding decision variables for problem 5 described in Table 2.

tion efficiency improves. However, as Figure 6b shows, X_{TBA} actually decreased with increasing eluent flow rate ($\gamma = 1.6$). This result can be easily understood when one observes that, with increasing eluent flow rate, both the raffinate and the extract flow rates increase, and therefore, more unconverted TBA is collected at this port before it is converted. This is particularly true for MTBE synthesis, as the reaction is kinetically controlled. The values of σ_{H_2O} reported in Table 4 show that the performances of sections P and R are greatly enhanced when γ is increased. This is particularly true for section R when $\gamma = 1.6$. σ_{H_2O} decreases to its desired value of less than 1 (0.77) for the first time in all of the cases studied. Therefore, increasing γ makes high MTBE purity possible, but at higher operating cost.

Effects of Column Length, L_{col}, and Total Number of Columns, N_{col}. The effects of the column length, L_{col}, and total number of columns, N_{col}, are shown in Figures 7 and 8, respectively. In Figure 7, the Pareto-optimal solutions for two different column lengths (L_{col} = 15 and 35 cm) are compared with the reference run solution (L_{col} = 25 cm), with the total number of columns, N_{col}, fixed at the reference value (see Table 2). In Figure 8, the optimization results are compared to see the effect of number of columns (N_{col} = 4, 6, and 8) with the length of the columns, L_{col}, fixed at 25 cm. As in the case of increasing Q_p, it was found that increasing the column length or number of columns has no effect on the shift of the Pareto. This is due to the high separation factor ($K_{H_2O}/K_{MTBE} = 9.17$) of the two reaction products. All of the decision variables were also unaffected, except for the switching time, which changed proportionately to preserve the same pseudo solid flow rate as shown in Figures 7f and 8f. This implies that the same results can be obtained with less catalyst (and adsorbent), the effect of which is studied later in case 2. However, when N_{col} was further decreased to 4 (i.e., only one column in each section), the optimal results deteriorated considerably, and it was found that no chromosomes could satisfy the constraint that X_{TBA} be greater 90% (see Figures 7b and 8b).

Effect of Operating Temperature *T*. The operating temperature influences the reaction kinetics, equilibrium conversion, and adsorption equilibrium (see the Appendix). For the MTBE synthesis reaction, higher temperatures result in an increase of the reaction rate but decreases in the equilibrium conversion and adsorption. The effects of operating temperature on the adsorption equilibrium constant and the reaction equi-

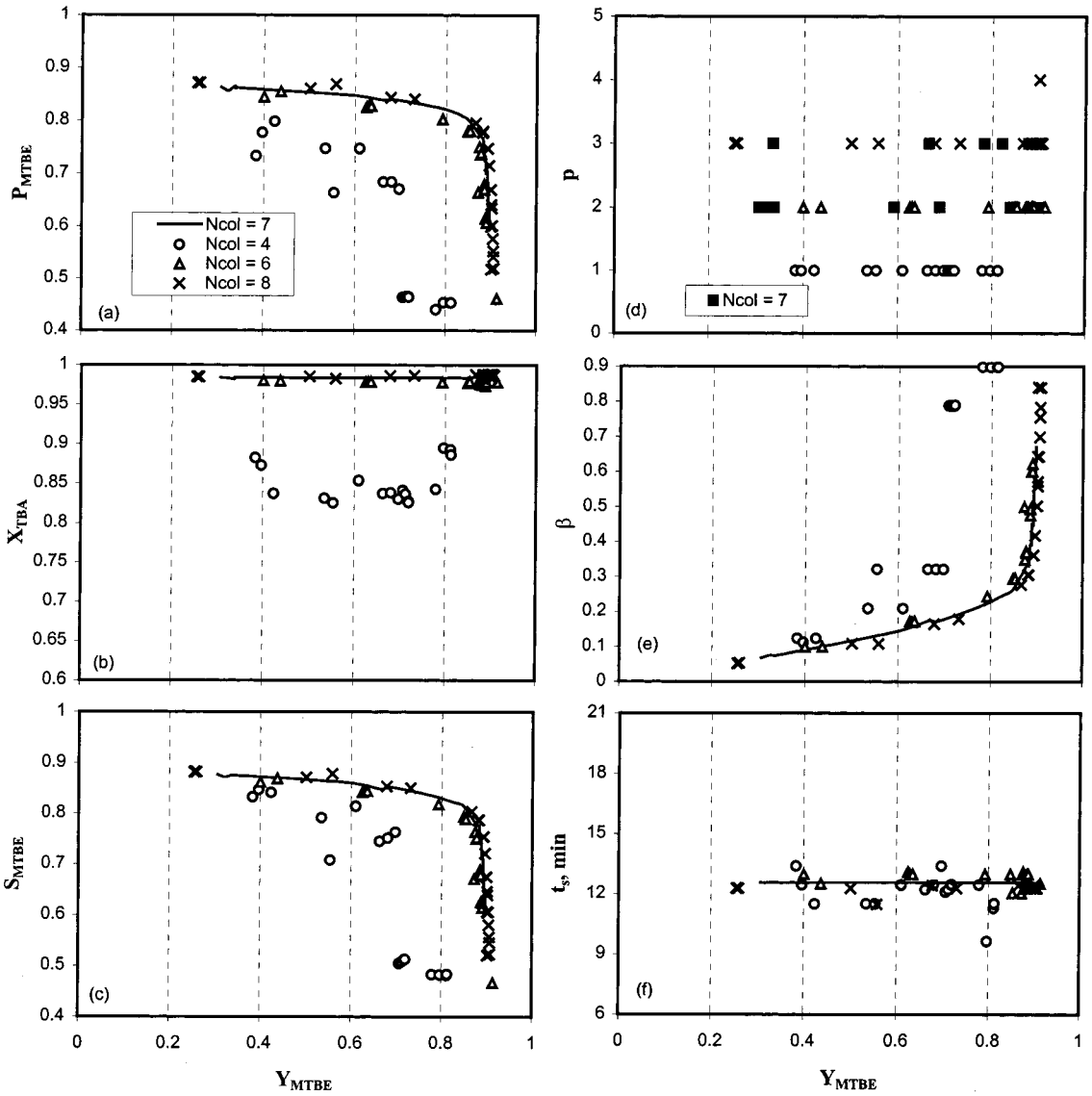

Figure 8. Effect of the total number of columns, N_{col}, on the Pareto and the corresponding decision variables for problem 6 described in Table 2.

librium constant are small compared to that on reaction rate parameter, k_f, in the range of 318−328 K. The reaction rate constant at 328 K is more than 4 times than that at 318 K. The effect of operating temperature on the optimization result is shown in Figure 9. The optimum solutions obtained (Pareto as well as the decision variables) at $T = 323$ K are same as those obtained in the reference run for $T = 328$ K. Although the reaction rate constant is lower at $T = 323$ K (compared to at 328 K), the system flow rates, column length, and total number of columns ensure enough retention time for an almost complete conversion of TBA. However, when the temperature was decreased further to 318 K, the reaction was so slow that more unconverted reactant (TBA) appeared at the raffinate and extract products. As a result, X_{TBA} decreased, as shown in Figure 9b. However, X_{TBA} (at 318 K) can be improved by reducing Q_p, thereby increasing the residence time for TBA, as shown (by symbol x in Figure 9) by the result at $T = 318$ K when $Q_p = 0.556$ mL/min. Surprisingly, Y_{MTBE} also improves for the same values of P_{MTBE}. The improvement can be illustrated by points 10 ($T = 318$ K, $Q_p = 1$ mL/min) and 11 ($T = 318$ K, $Q_p = 0.556$ mL/min) shown in Figure 9. Table 3 shows that point 11 has almost the same P_{MTBE} value as point 10; however, its Y_{MTBE} value reaches 95.57% compared to 90.27% at point 10. As discussed earlier, the improvement in Y_{MTBE} is due to the better performance of sections Q and S in preventing the loss of MTBE in the extract stream. This can be seen in Table 4 from the σ values reported for the two sections.

Case 2. Maximization of Y_{MTBE}/V_{solid} and P_{MTBE}/V_{solid}

The first optimization problem (case 1) aimed at maximizing the yield and purity of MTBE for an existing SCMCR setup. However, optimization at the design stage provides far more freedom than than optimization of the performance of an existing system. At the design stage, several additional decision (or design) variables become available for optimization. A meaningful optimization problem could be the following

$$\max J_1 = Y_{MTBE}/V_{solid}(t_s,\beta,p,q,r,s,L_{col}) \quad (10a)$$

$$\max J_2 = P_{MTBE}/V_{solid}(t_s,\beta,p,q,r,s,L_{col}) \quad (10b)$$

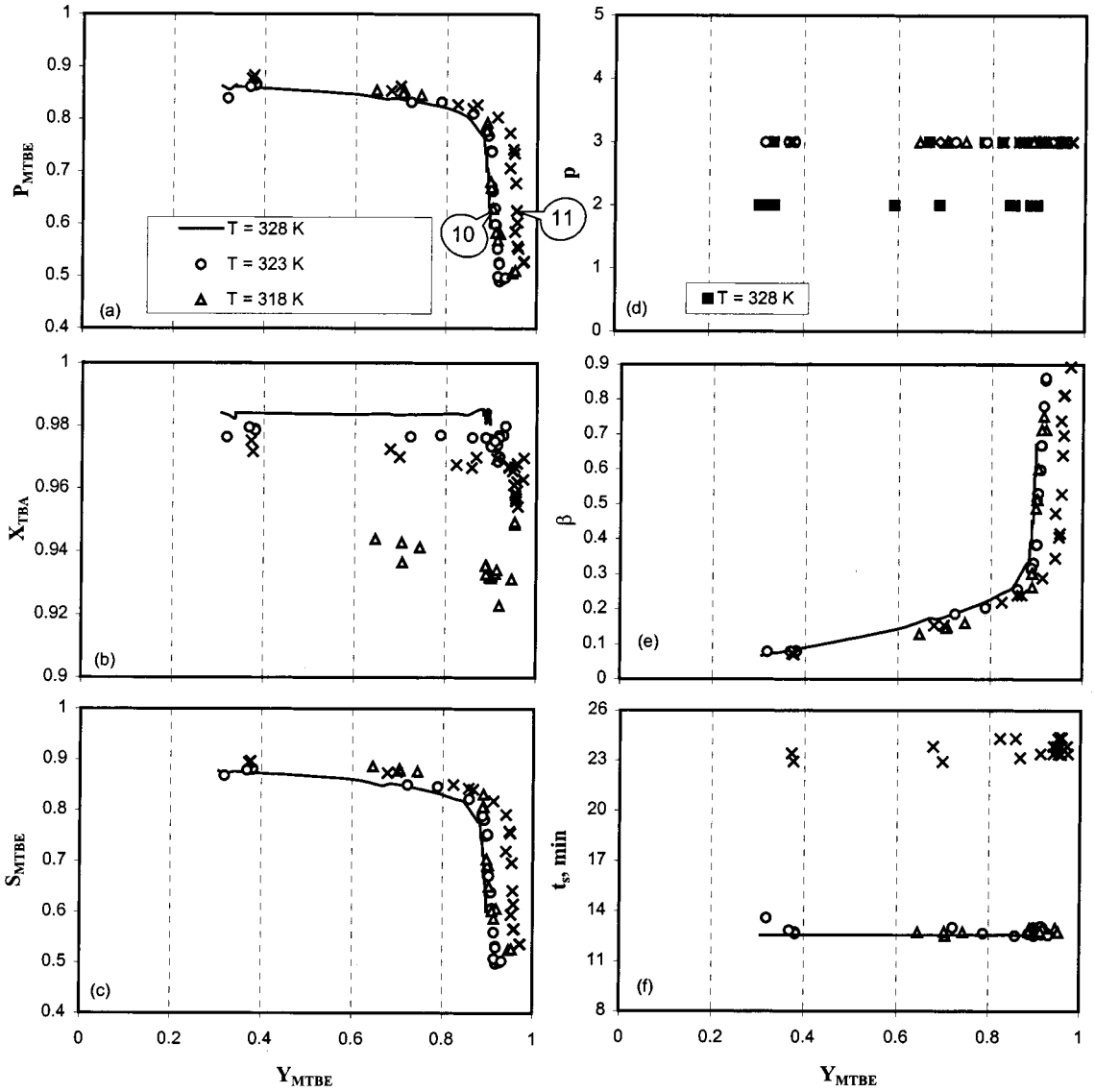

Figure 9. Effect of the operating temperature, *T*, on the Pareto and the corresponding decision variables for problem 7 described in Table 2.

subject to

$$X_{TBA} \geq 90\% \tag{10c}$$

$$\alpha = 0.1,\ \gamma = 0.8,\ Q_p = 1\ \text{mL/min},\ d_{col} = 0.94\ \text{cm},\ T = 328\ \text{K} \tag{10d}$$

$$\text{model eqs described in the Appendix} \tag{10e}$$

The objective functions selected for this case are minimization of the total volume of the stationary phase required to achieve the maximum possible yield and purity of MTBE at the raffinate port all at once. Of course, we could have selected an optimization problem involving three objective functions rather than only two objective functions, similar to one reported recently by Oh et al.[29] for an industrial hydrogen plant. However, analysis of a three-objective-function Pareto becomes difficult, as one has to examine surfaces instead of lines. Hence, we used a combination of the two objective functions defined in eqs 10a and 10b, which will simultaneously minimize V_{solid} and maximize Y_{MTBE} and P_{MTBE}. V_{solid} is defined as

$$V_{solid} = \frac{\pi}{4} d_{col}^2 L_{col} N_{col} = \frac{\pi}{4} d_{col}^2 L_{col}(p + q + r + s) \tag{11}$$

In case 2, therefore, we allowed the number of columns (*p*, *q*, *r*, and *s*) in each section (P, Q, R, and S) to vary between 1 and 3 (see Table 5) while simultaneously determining the optimal length of each column. Hence, in this case, there are seven decision variables instead of three for case 1. The complete optimization formulation for case 2, along with the bounds on the decision variables and the fixed parameter values used, is described in Table 5. The optimal design of the SCMCR is explored to maximize Y_{MTBE} and P_{MTBE} and minimize V_{solid} for a fixed solvent usage (eluent consumption) and throughput (feed rate, α) and a maximum allowable pressure drop (flow rate, Q_p).

The optimal solutions obtained are shown in Figures 10 and 11. Figure 10 compares the optimal Pareto solution for three runs, one where L_{col} was fixed at 25 cm (reference run, case 1) and two other runs where the lower bounds for L_{col} used were 15 and 18 cm. Because V_{solid} is minimized in this case, the (Y_{MTBE}/V_{solid}) − (P_{MTBE}/V_{solid}) Pareto curve shifts upward with decreasing optimum L_{col}. Therefore, incorporating V_{solid}

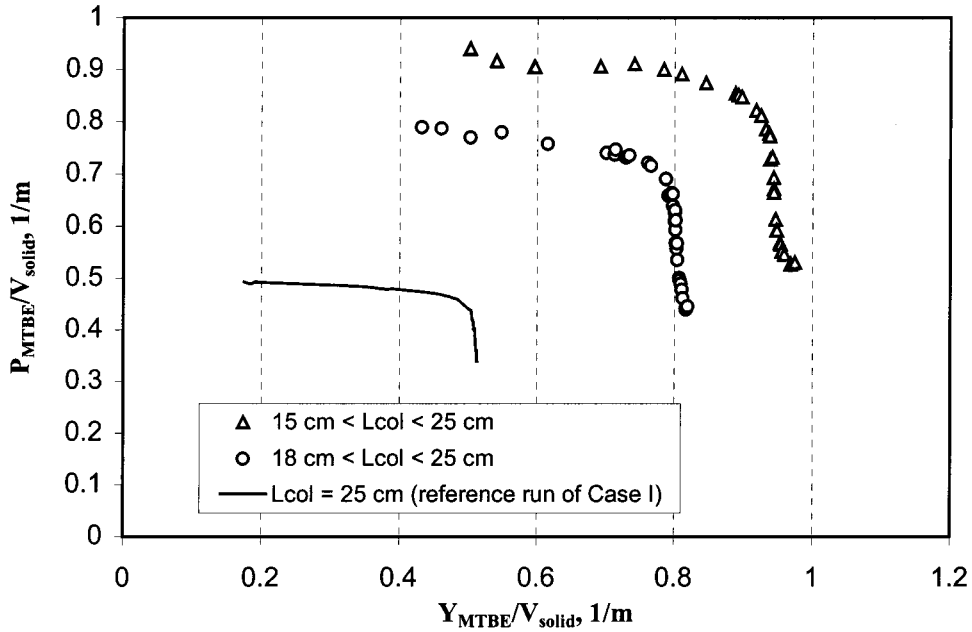

Figure 10. Pareto set for case 2 optimization problem described in Table 5.

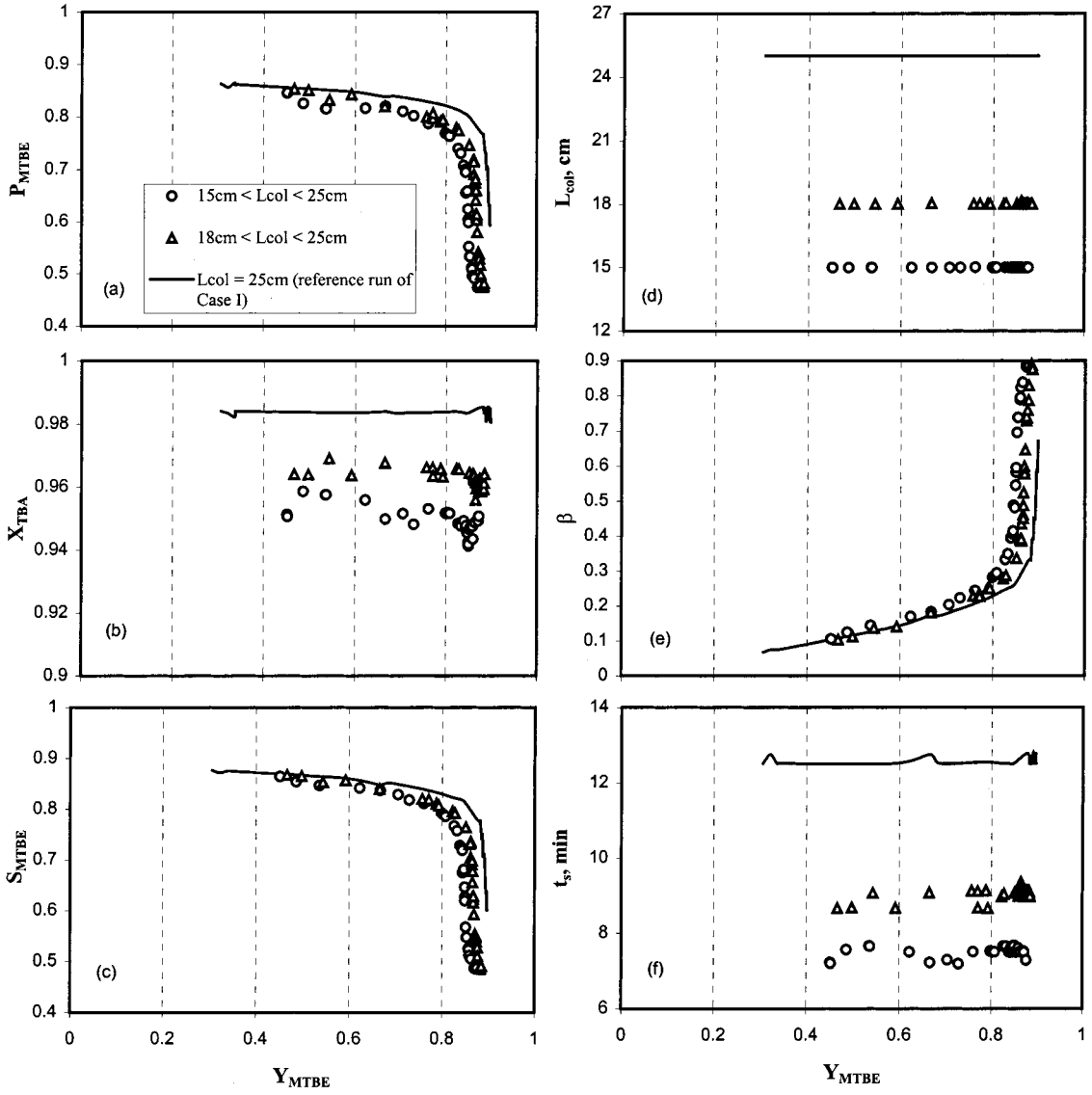

Figure 11. Values of P_{MTBE}, S_{MTBE}, X_{TBA}, and the decision variables (L_{col}, β, t_s) corresponding to the points on the Pareto set in Figure 10.

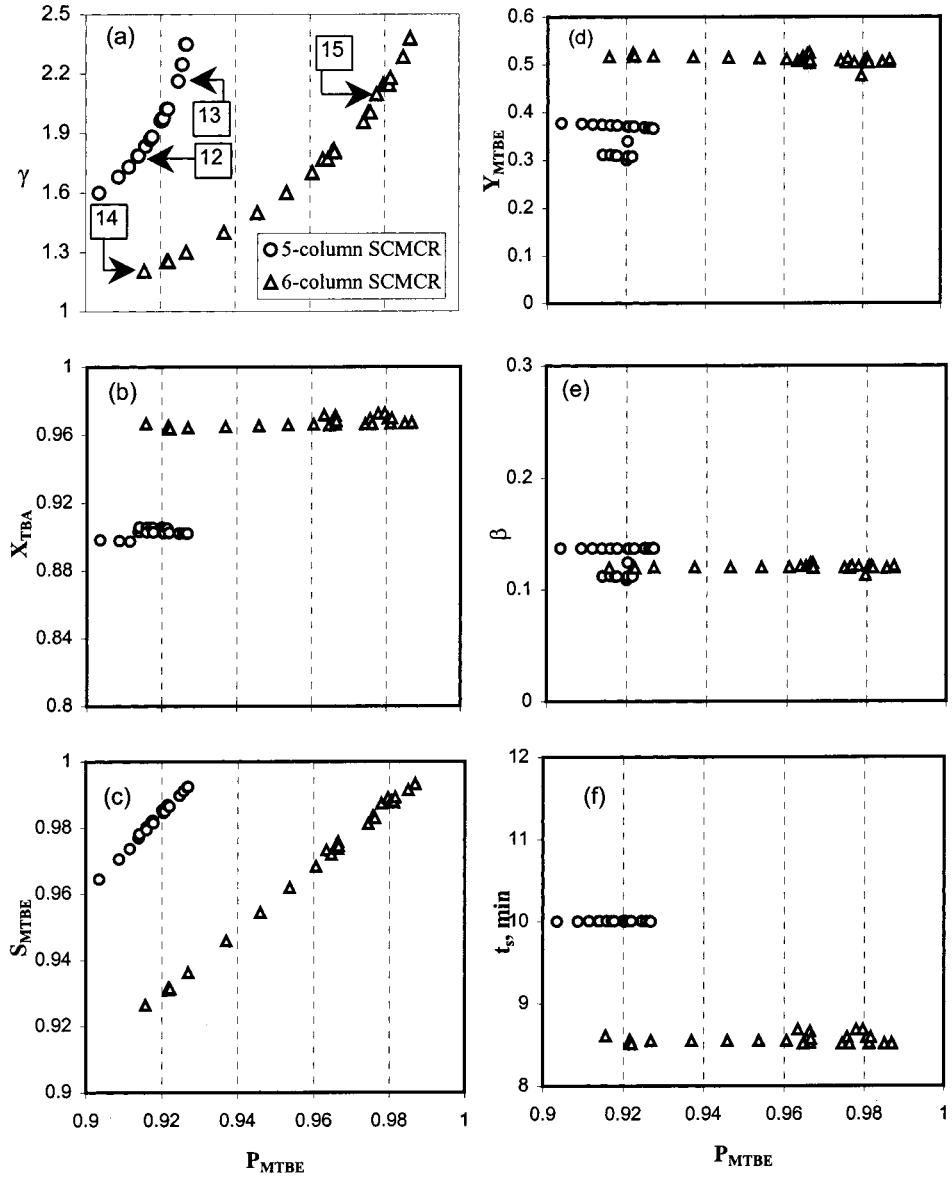

Figure 12. Pareto set for case 3 optimization problem described in Table 5 and corresponding values of X_{TBA}, S_{MTBE}, Y_{MTBE}, and the decision variables (β, t_s) corresponding to the points on the Pareto set in Figure 11a.

Table 5. Description of the Other Optimization Problems Solved in This Study Together Bounds of Decision Variables

case	objective function	constraint	decision variables	fixed parameters
2	max Y_{MTBE}/V_{solid} max P_{MTBE}/V_{solid}	$X_{TBA} \geq 90\%$	$4 < t_s < 20$ min $0.10 \leq \beta \leq 0.90$ $1 \leq p, q, r, s \leq 3$ 15 (or 18) $< L_{col} < 25$ cm	$\alpha = 0.1$, $\gamma = 0.8$, $Q_p = 1$ mL/min, $d_{col} = 0.94$ cm, $T = 328$ K
3	max P_{MTBE} min γ	$X_{TBA} \geq 90\%$	$4 < t_s < 20$ min $0.10 \leq \beta \leq 0.90$ $1 \leq p, q, r \leq 3$ $1 < \gamma < 2.5$	$\alpha = 0.1$, $Q_p = 1$ mL/min, $N_{col} = 5$ or 6, $L_{col} = 18$ cm, $d_{col} = 0.94$ cm, $T = 328$ K

into the objective function helps to increase the efficiency of the catalyst (adsorbent) usage. P_{MTBE}, X_{TBA}, S_{MTBE}, and the decision variables (L_{col}, β and t_s) corresponding to all points in Figure 10 are shown as a function of Y_{MTBE} in Figure 11. The variables are plotted against Y_{MTBE} on the x axis rather than the objective function used (Y_{MTBE}/V_{solid}) for convenience of comparison. The optimal number of columns (N_{col}) was found to be 6, and the optimal column distribution was 2, 1, 1, and 2 columns for sections P, Q, R, and S, respectively. Therefore, the assumption made in case 1 that one column each is sufficient for sections Q and R based on the sensitivity study (Table 1) was found to be correct. Furthermore, the optimal value of the decision variable, L_{col}, was found to hit the lower bound for each run, as shown in Figure 11d, to minimize V_{solid}. Therefore, a significant reduction in the amount of adsorbent (resin) can be achieved over the reference run (case 1, where $N_{col} = 7$, $L_{col} = 25$ cm) for an almost identical purity and yield of MTBE. For example, in case 2, a ~48.6% reduction in V_{solid} is achieved for optimum values of L_{col} and N_{col} equal to 15 cm and 6, respectively. The effect of L_{col} and N_{col} on P_{MTBE} and Y_{MTBE} has already been found to be insignificant for case 1

Table 6. Adsorption Constants K_i; Kinetic Parameters k_f, K_e, and n; and Dispersion Coefficients D_i[3]

T (K)	K_{MTBE}	K_{H_2O}	K_{TBA}	k_f [mol$^{(1-n)}$L$^{(n-1)}$/min]	K_e (mol/L)	n	$10^6\ D_{MTBE}$ (m^2/s)	$10^6\ D_{H_2O}$ (m^2/s)
318	0.375	2.846	0.460	0.025	24.682	1.018	1.948	7.092
323	0.330	2.800	0.440	0.060	20.943	1.092	2.333	7.708
328	0.300	2.750	0.460	0.112	18.202	1.120	2.350	8.167

optimization (Figures 7 and 8). Hence, when V_{solid} was minimized (case 2), it was found that, even though the purity decreased by about 5%, there was a significant savings in the amount of V_{solid}. The decrease in X_{TBA} in Figure 11b can be explained by the decrease in the residence time of TBA; as a result, less TBA is converted to MTBE, and Y_{MTBE} decreases. A higher raffinate flow β is required to maintain the same value of Y_{MTBE} as in the reference run, as shown in Figure 11e, but at a sacrifice in P_{MTBE}.

Case 3. Maximization of P_{MTBE} and Minimization of γ

The third optimization problem (case 3) solved in this study was maximization of the purity of MTBE (P_{MTBE}) with simulataneous minimization of the eluent consumption (γ) for a given productivity (α), and existing setup (fixed N_{col} and L_{col}). The optimization problem solved in case 3 is described in Table 5. The choice of the two objective functions enabled the production of pure MTBE at the raffinate port using the minimum amount of eluent. Figure 12 compares the optimal Pareto solutions obtained with five-column and six-column SCMCRs. Figure 12a shows that (a) more eluent is needed to obtain a high P_{MTBE} and (b) a six-column system either requires less eluent for the same desired P_{MTBE} or can obtain a much higher P_{MTBE} for the same eluent flow rate compared to a five-column SCMCR. The values of X_{TBA}, S_{MTBE}, and Y_{MTBE} and decision variables (β and t_s) corresponding to all points in Figure 12a are shown against P_{MTBE} in Figure 12b−f. The optimal column distributions obtained in this case for sections P, Q, R, and S, respectively, are 2, 1, 1, and 1 for the five-column SCMCR and 2, 1, 1, and 2 for the six-column SCMCR. It can easily be seen that, to increase P_{MTBE}, we need to place the extra column in section P to increase the residence time for separation of MTBE and H_2O for the five-column SCMCR, whereas for the six-column SCMCR, the additional column must be placed in section S to increase the recycle of MTBE contaminated with less H_2O to further increase P_{MTBE}.

Conclusions

Integrated reactor−separators based on simulated moving-bed (SMB) technology have received great attention in recent years. Countercurrent movement of the solids is mimicked in SMBs by switching the inlet and outlet ports in unison at fixed predetermined switching times. In this paper, we presented a systematic study for the optimal operation of an SCMCR for the direct synthesis of MTBE from *tert*-butyl alcohol and methanol. We developed a mathematical model for the MTBE synthesis reaction in an SCMCR. The model was solved using experimentally determined kinetic and adsorption parameters. It was found that the selection of operating parameters for the SCMCR such as the length and number of columns, switching time interval, and liquid flow rates in different sections is not straightforward. In most cases, conflicting requirements and constraints govern the optimal choice of the decision (operating or design) variables. The economical operation of an SCMCR process is governed by many factors depending on the objective and the product quality. One might be interested in producing a high purity of MTBE using minimum solvent (eluent) or in producing as high a purity as possible for MTBE while at the same time maximizing the yield of MTBE. In this paper, we considered three multiobjective optimization problems involving the simultaneous optimization of more than one objective functions. Optimal designs and operating conditions were found for the three cases: (a) simultaneous maximization of the purity and yield of MTBE, (b) minimization of the amount of catalyst/adsorbent required together with simultaneous maximization of the purity and yield of MTBE, and (c) maximization of the purity of MTBE with simultaneous minimization of the eluent consumption, in the presence of meaningful constraints for better product quality. The optimization was performed using a very robust, state-of-the-art AI-based technique, the nondominated sorting genetic algorithm (NSGA). A Pareto-optimal curve, which provides a set of optimal solutions that are equally good, was obtained. It was found that optimal performance of the SCMCR could be better in terms of producing high-purity MTBE using either less eluent or less adsorbent/catalyst or at the same time achieving a better yield of MTBE. It should be emphasized that there is no end to the variety of multiobjective optimization problems that could be formulated and studied, and we presented only a few simple examples here to illustrate the concepts, techniques, and interpretation of results. To the best of our knowledge, this is the first attempt at addressing such a problem for simulated countercurrent moving-bed chromatographic reactor (SCMCR) systems.

Notation

C = liquid-phase concentration, mol/l
D = apparent axial dispersion coefficient, m^2/s
k = reaction rate constant
K = equilibrium constant
L = length of column, m
n = number of moles of TBA reacted per mole of methanol
p = number of columns in section P
P = purity
q = concentration in the polymer phase, mol/l; number of columns in section Q
Q = volumetric flow rate, m^3/s
r = number of columns in section R
R = reaction rate, mol/(min L)
s = number of columns in section S
S = selectivity
t = time, s
T = temperature, K
u = superficial velocity, m/s

V = velocity, m/s
X = conversion
Y = yield
z = axial coordinate, m

Greek Letters

α = fraction of feed
β = fraction of raffinate withdrawn
γ = fraction of eluent
δ = phase ratio
ϵ = void fraction
ϕ = section
σ = relative carrying capacity
ζ = pseudo solid-phase velocity
ν = stoichiometric coefficient of component

Subscripts/Superscripts

o = initial, inlet
b = backward
e = equilibrium
f = feed, forward
g = gas, carrier
i = component i
j = column j
s = solid, switching
N = number, switching period

Appendix: Complete Set of Equations for the Mathematical Model of the SCMCR Used in This Work and Described in Detail in Zhang et al.[4]

The material balance for component i in the jth column during the Nth switching period is given by

$$\frac{\partial C_{ij}^{(N)}}{\partial t} + \left(\frac{1-\epsilon}{\epsilon}\right)\frac{\partial q_{ij}^{(N)}}{\partial t} + \frac{u_\phi}{\epsilon}\frac{\partial C_{ij}^{(N)}}{\partial z} - \left(\frac{1-\epsilon}{\epsilon}\right)\nu_i R_j^{(N)} = D_i\frac{\partial^2 C_{ij}^{(N)}}{\partial z^2} \quad \text{(A1)}$$

where i = TBA, MTBE, or H_2O; u_ϕ designates the superficial flow rate in section ϕ (where ϕ = P, Q, R, or S), and the reaction rate and adsorption isotherm are given by

$$R_j^{(N)} = k_f\left(q_{TBA,j}^{n(N)} - \frac{q_{MTBE,j}^{(N)}\, q_{H_2O,j}^{n(N)}}{K_e}\right) \quad \text{(A2)}$$

$$q_{ij}^{(N)} = K_i C_{ij}^{(N)} \quad \text{(A3)}$$

The initial and boundary conditions are as follows

Initial conditions

$$\text{when } N = 0, \quad C_{ij}^{(0)} = C_{ij}^{\text{initial}} = 0 \quad \text{(A4)}$$

$$\text{when } N \geq 1, \quad C_{ij}^{(N)} = C_{i,j+1}^{(N-1)} \quad \text{for } j = 1, ..., (N_{col} - 1)$$

$$C_{ij}^{(N)} = C_{i1}^{(N-1)} \quad \text{for } j = N_{col} \quad \text{(A5)}$$

Boundary conditions

Feed point (point A)

$$C_{i1}^{(N)}|_{z=0} = (1-\alpha)C_{i,N_{col}}^{(N)}|_{z=L} + \alpha C_{i,f} \quad \text{(A6)}$$

Raffinate withdrawal point (point B)

$$C_{i,p+1}^{(N)}|_{z=0} = C_{i,p}^{(N)}|_{z=L} \quad \text{(A7)}$$

Eluent inlet point (point C)

$$C_{i,p+q+1}^{(N)}|_{z=0} = \left(\frac{1-\beta}{1-\beta+\gamma}\right)C_{i,p+q}^{(N)}|_{z=L} \quad \text{(A8)}$$

Extract withdrawal point (point D)

$$C_{i,p+q+r+1}^{(N)}|_{z=0} = C_{i,p+q+r}^{(N)}|_{z=L} \quad \text{(A9)}$$

The mass balance equation (eq A1), initial (eqs A4 and A5) and boundary (eqs A6−A9) conditions, kinetic equation (eq A2), and adsorption isotherm (eq A3) completely define the SCMCR system. After each switching, the column numbering was redefined according to eq A10 so that the feed was always introduced into the first column.

$$\begin{bmatrix} \text{before switching} & \text{after switching} & \\ \text{column 1} & \text{column } N_{col} & \\ \text{column } j & \text{column } j-1 & j = 2, 3, ..., N_{col} \end{bmatrix} \quad \text{(A10)}$$

The adsorption constants K_i; kinetic parameters k_f, K_e, and n; and dispersion coefficients D_i were obtained from ref 3 and are given in Table 6.

Literature Cited

(1) Ray, A. K.; Carr, R. W.; Aris, R. The simulated countercurrent moving-bed chromatographic reactor—A novel reactor separator. *Chem. Eng. Sci.* **1994**, *49* (4), 469−480.

(2) Ray, A K.; Carr, R. W. Numerical simulation of a simulated countercurrent moving bed chromatographic reactor. *Chem. Eng. Sci.* **1995**, *50* (19), 3033−3041.

(3) Zhang, Z.; Hidajat, K.; Ray, A. K. Determination of adsorption and kinetic parameters for methyl *tert*-butyl ether synthesis from *tert*-butyl alcohol and methanol. *J. Catal.* **2001**, *200* (2), 209.

(4) Zhang, Z.; Hidajat, K.; Ray, A. K. Application of simulated countercurrent moving bed chromatographic reactor for MTBE synthesis. *Ind. Eng. Chem. Res.* **2001**, *40* (23), 5305.

(5) Holland, J. H. *Adaptation in Natural and Artificial Systems: An Introductory Analysis with Applications to Biology, Control and Artificial Intelligence*; University of Michigan Press: Ann Arbor, MI, 1975.

(6) Goldberg, D. E. *Genetic Algorithms in Search, Optimization, and Machine Learning*; Addison-Wesley: Reading, MA, 1989.

(7) Deb, K. *Optimization for Engineering Design: Algorithms and Examples*; Prentice Hall of India: New Delhi, India, 1995.

(8) Deb, K. *Multiobjective Optimization Using Evolutionary Algorithms*; John Wiley & Sons: New York, 2001.

(9) Chankong V.; Haimes, Y. Y. *Multiobjective Decision Making—Theory and Methodology*; Elsevier: New York, 1983.

(10) Fonseca, C. M.; Fleming, P. J. Multiobjective optimization and multiple constraint handling with evolutionary algorithms. Part I: A unified formulation. *IEEE Trans. Syst., Man, Cybernetics* **1998**, *A28*, 26.

(11) Srinivas, N.; Deb, K. Multiobjective optimization using nondominated sorting in genetic algorithms. *Evol. Comput.* **1995**, *2*, 106.

(12) Bhaskar, V.; Gupta, S. K.; Ray, A. K. Applications of multiobjective optimization in chemical engineering. *Rev. Chem. Eng.* **2000**, *16*, 1.

(13) Mitra, K.; Deb, K.; Gupta, S. K. Multiobjective dynamic optimization of an industrial nylon 6 semi-batch reactor using genetic algorithm. *J. Appl. Polym. Sci.* **1998**, *69*, 69.

(14) Bhaskar, V.; Gupta, S. K.; Ray, A. K. Multiobjective optimization of an industrial wiped film poly(ethylene terephthalate) reactor. *AIChE J.* **2000**, *46* (5), 1046.

(15) Bhaskar, V.; Gupta, S. K.; Ray, A. K. Multiobjective optimization of an industrial wiped film poly(ethylene terephthalate) reactor: Some further insights. *Comput. Chem. Eng.* **2001**, *25*, 391.

(16) Zhou, F.; Gupta, S. K.; Ray, A. K. Multiobjective optimization of the continuous casting process for poly(methyl methacrylate) using adapted genetic algorithm. *J. Appl. Polym. Sci.* **2000**, *78*, 1439.

(17) Rajesh, J. K.; Gupta, S. K.; Rangaiah, G. P.; Ray, A. K. Multiobjective optimization of steam reformer performance using genetic algorithm. *Ind. Eng. Chem. Res.* **2000**, *39* (3), 706.

(18) Rajesh, J. K.; Gupta, S. K.; Rangaiah, G. P.; Ray, A. K. Multi-objective optimization of industrial hydrogen plants. *Chem. Eng. Sci.* **2001**, *56* (3), 999.

(19) Ravi, G.; Gupta, S. K.; Ray, M. B. Multiobjective optimization of cyclone separators. *Ind. Eng. Chem. Res.* **2000**, *39* (11), 4272.

(20) Yuen, C. C.; Aatmeeyata; Gupta, S. K.; Ray, A. K. Multiobjective optimization of membrane separation modules using genetic algorithm. *J. Membr. Sci.* **2000**, *176* (2), 177.

(21) Petroulas, T.; Aris, R.; Carr, R. W. Analysis and performance of a countercurrent moving-bed chromatographic reactor. *Chem. Eng. Sci.* **1985**, *40*, 2233.

(22) Fish, B.; Carr, R. W.; Aris, R. The continuous countercurrent moving bed chromatographic reactor. *Chem. Eng. Sci.* **1986**, *41* (4), 661.

(23) Ray, A K.; Tonkovich, A.; Carr, R. W.; Aris, R. The simulated countercurrent moving-bed chromatographic reactor. *Chem. Eng. Sci.* **1990**, *45* (8), 2431.

(24) Ray, A K.; Carr, R. W. Experimental study of a laboratory-scale simulated countercurrent moving bed chromatographic reactor. *Chem. Eng. Sci.* **1995**, *50* (14), 2195.

(25) Hashimoto, K.; Adachi, S.; Noujima, H.; Maruyama, A. Models for separation of glucose−fructose mixture using a simulated moving bed adsorber. *J. Chem. Eng. Jpn.* **1983**, *16*, 400.

(26) Ruthven, D. M. The axial dispersed plug flow model for continuous counter-current adsorbers. *Can. J. Chem. Eng.* **1983**, *61*, 881.

(27) Mazzotti, M.; Kruglov, A.; Neri, B.; Gelosa, D.; Morbidelli, M. A continuous chromatographic reactor: SMBR. *Chem. Eng. Sci.* **1996**, *51* (10), 1827.

(28) Dünnebier, G.; Fricke, J.; Klatt, K. U. Optimal design and operation of simulated moving bed chromatographic reactors. *Ind. Eng. Chem. Res.* **2000**, 39, 2290.

(29) Oh, P. P.; Ray, A. K.; Rangaiah, G. P. Triple objective optimization of industrial hydrogen plants. *J. Chem. Eng. Jpn.* **2001**, *34* (11), 1341.

Received for review August 21, 2001
Revised manuscript received March 13, 2002
Accepted April 9, 2002

IE0106940